https://doi.org/10.5194/egusphere-2026-6324
Preprint. Discussion started: 26 November 2026
© Author(s) 2026. CC BY 4.0 License.

Contrasting thermal dynamics of adjacent Greenlandic ice-marginal lakes

Peter A. Tuckett[1], Connie M. Harpur[2], Alex C. Scoffield[2], Duncan J. Quincey[2], Christopher J. Merchant[3,4], R. Iestyn Woolway[5], Hannah F. Barnett[2], Joseph Mallalieu[6], Lauren D. Rawlins[2], Joshua Abrahams[7], Jenna L. Sutherland[8], Laura Carrea[3], Niall McCarroll[3], Weijia Wang[5], David M. Rippin[1]

[1] Department of Environment & Geography, University of York, UK
[2] School of Geography and water@leeds, University of Leeds, UK
[3] Department of Meteorology, University of Reading, UK
[4] National Centre for Earth Observation, University of Reading, UK
[5] School of Ocean Sciences, Bangor University, UK
[6] School of Geography, Earth & Environmental Sciences, University of Birmingham, UK
[7] Faculty of Science & Engineering, University of Swansea, UK
[8] School of Built Environment, Engineering and Computing, Leeds Beckett University, UK

Correspondence to: Peter A. Tuckett (pete.tuckett@york.ac.uk)

Abstract. Approximately 10% of the Greenland Ice Sheet margin is fringed by ice-marginal lakes. The presence of lakes introduces the potential for enhanced ice-mass loss via subaqueous melt and calving, with impacts on ice dynamics and ice-margin retreat rate. Historically, it has been assumed that such lakes are uniformly cold, yet lake temperature measurements from Greenland are sparse. The importance of lake temperatures on ice sheet mass loss therefore remains unclear. Here, we present continuous in-situ time series of depth-resolved water temperature from three lakes on the western margin of the Greenland Ice Sheet, collected between July 2024 and August 2025. By combining sub-hourly lake temperature measurements with meteorological, lake turbidity and time-lapse camera data, we investigate sub-diurnal to seasonal influences on lake thermal dynamics. Ice-marginal lake surface temperatures reached highs greater than 8 °C, while water temperatures often exceeded 4 °C throughout the entire water column during summer months. Summer warm-surface stratification persisted for several weeks, whilst inverse stratification occurred when surface water temperatures dropped below 4 °C. We observed contrasting summer and winter thermal regimes between two adjacent ice-marginal lakes, which we attribute to differences in subglacial meltwater input. Our findings demonstrate that ice-marginal lake thermal characteristics are highly variable and suggest that subaqueous melt rates in some ice-marginal settings may be substantially higher than previously assumed. Enhanced in-situ monitoring of lake thermal characteristics and consideration of lake-specific subglacial meltwater inputs are therefore necessary to accurately parameterise lake temperatures in ice-sheet evolution models.

https://doi.org/10.5194/egusphere-2026-6324
Preprint. Discussion started: 26 November 2026
© Author(s) 2026. CC BY 4.0 License.

1 Introduction

The Greenland Ice Sheet has been losing mass at an increasing rate since the early 1990s, primarily due to increased surface melting associated with climate warming (Hanna et al., 2026). One notable consequence of this increased surface meltwater runoff has been an increase in the number and size of ice-marginal lakes: lakes in contact with the ice sheet margin, which typically form when meltwater accumulates behind moraines or in newly exposed over-deepened basins. At present, over 2900 lakes are in direct contact with the ice sheet (How et al., 2025), occupying around ~10% of the ice sheet margin (Carrivick et al., 2022). However, progressive ice sheet margin recession means the number and size of ice-marginal lakes is increasing (Carrivick & Quincey, 2014; How et al., 2021), with this trend expected to continue during the coming decades (Carrivick et al., 2022). This is potentially important for future ice sheet mass balance because ice-marginal lakes can influence ice dynamics and ice margin recession rates (Mallalieu et al., 2021; Vacek et al., 2026). In particular, thermo-mechanical processes at the lake-ice interface promote subaqueous melt and calving, whilst buoyancy-driven reductions in basal drag and longitudinal buttressing can cause ice flow accelerations (Warren & Kirkbride, 2003; Sutherland et al., 2020; Minowa et al., 2023). As a result of these processes, ice velocities at Greenlandic lake-terminating outlet glacier termini are, on average, three times greater than at equivalent land-terminating margins (Harpur et al., 2026), whilst the presence of lakes has been shown to enhance ice sheet retreat (Mallalieu et al., 2021). Despite this, ice-marginal lake processes are mostly omitted from current ice sheet evolution models (Carrivick et al., 2020), partly due to a lack of empirical data upon which to base parameterisations of ice-lake interactions. Ice-marginal lakes hence represent a known, yet unquantified, source of uncertainty in projections of Greenlandic contribution to future sea level rise.

A potentially important yet currently poorly constrained control on ice-marginal lake influence is lake temperature. Small ice-marginal lakes have traditionally been considered to be uniformly cold (<1 °C), resulting in low subaqueous melt rates (Truffer & Motyka, 2016). However, growing global evidence indicates that ice-marginal lakes of all sizes can be relatively warm and thermally variable. Ice-marginal lake temperatures greater than 4 °C have been reported in locations including Patagonia (Sugiyama et al., 2016, 2021), Arctic Sweden (Dye et al., 2025), New Zealand (Warren & Kirkbride, 1998; Röhl, 2006) and Nepal (Watson et al., 2020; Scoffield et al., 2025), whilst remote sensing studies of Greenlandic lakes have reported maximum surface temperatures of 10 °C in large ice-marginal lakes (Carrea et al., 2025). The 4 °C threshold is significant because it roughly marks the temperature of maximum freshwater density (3.98 °C), enabling vertical stratification provided lakes are sufficiently deep and there is limited wind-driven mixing (Boehrer & Schultze, 2008). Stratification concentrates solar heating in a shallower layer which amplifies maximum temperatures at the lake surface, enhancing lake-level and subaqueous melt. Relatively warm water at the lake-ice interface can thus cause thermal undercutting of the ice front, resulting in overhanging subaerial ice cliffs and increasing the likelihood of calving (Kirkbride & Warren, 1998). Spatially focused melt under stratified conditions can also produce a submerged ice foot, exerting an upward buoyant force that destabilises the terminus and promotes buoyancy-driven calving (Warren et al., 2001; Sugiyama et al., 2019). These stratification-driven processes exert an important

https://doi.org/10.5194/egusphere-2026-6324
Preprint. Discussion started: 26 November 2026
© Author(s) 2026. CC BY 4.0 License.

control on seasonal and interannual rates of calving and retreat in locations including Arctic Sweden (Dye et al., 2025) and Patagonia (Minowa et al., 2017), and could be more common in Greenland than currently realised (Mallalieu et al., 2020).

Previous studies of Greenlandic ice-marginal lake temperatures are sparse. Satellite data have been used to derive lake surface temperature estimates of selected individual lakes (Carrea et al., 2025) and Greenland-wide lake inventories (How et al., 2025), but a lack of in-situ validation makes it difficult to assess the uncertainty of these data (How et al., 2025). Furthermore, satellite data provide no direct measurements of sub-surface lake temperatures and vertical thermal structure. In-situ lake temperature measurements have predominantly been collected at non-glacially fed lakes in west Greenland, often with a limnological (Kettle et al., 2004; Saros et al., 2016) or ecological focus (Greenland Ecosystem Monitoring, 2020). Burpee et al. (2018) report point-based surface lake temperature measurements from four glacially-fed lakes, two of which were ice-contact, but measurements were taken near to shore, so are unlikely to be representative of lake-wide temperatures. A recent study by Vacek et al. (2026) reports year-round temperatures from a single probe at ~5 m depth in a large ice-marginal lake in southern Greenland. Prior to this, six other Greenlandic lakes were reported to have continuous in-situ measurements (How et al., 2025). However, only one of these lakes (Russell Lake, 67°08'17"N 50°04'32"W) is in contact with the ice sheet, with temperature data limited to the summer months and restricted to either surface or lake bed (Carrivick et al., 2017) measurements. To our knowledge, no long-term, multi-depth temperature profile data from Greenlandic ice-marginal lakes have been recorded.

In this study, we provide the first in-situ, high resolution, continuous time series of Greenlandic ice-marginal lake water temperatures. We present laterally and vertically distributed thermistor data from two neighbouring ice-marginal lakes, and one non-glacially-fed lake for comparison, between July 2024 and August 2025. We analyse our lake temperature dataset in combination with meteorological data, turbidity data, and timelapse camera imagery, enabling an assessment of the controls on lake temperature variability and changes in thermal structure.

2 Study Region

Fieldwork was conducted at three unnamed lakes south-east of Leverett Glacier in south-west Greenland: two ice-marginal lakes, hereafter named ‘Ice-marginal 1’ (IML-1, 67°03'48"N 50°03'16"W) & ‘Ice-marginal 2’ (IML-2, 67°02'57"N 50°01'31"W), and one non-glacially fed lake (NGL, 67°03'09"N 50°07'44"W) as a control (Fig. 1). South-west Greenland has experienced rapid warming since the early 1990s, resulting in a ~1% increase in surface melt per year (Hanna et al., 2026) and a 75% increase in the number of ice-marginal lakes (How et al., 2021). IML-1 and IML-2 are broadly representative of regional lake sizes (mean ice-marginal lake area in south-west Greenland is 1.1 km^2; How et al., 2021) and are situated in a hydrologically dynamic region with potential for subglacial meltwater input (Clason et al., 2015; Ross et al., 2018). Both lakes are fed by ice flow of ~50-80 m yr^{-1} (Gardner et al., 2025) and have active calving fronts.

The three study lakes lie at elevations of 509 m above sea level (IML-1), 447 m asl (IML-2), and 415 m asl (NGL) respectively. IML-1 has an area of 0.40 km^2, a single ~375 m wide calving front, and a quasi-rectangular geometry (Fig. 1). The lake has a single, ~6 m wide outflow channel at its ice distal end, which flows into an intermediary lake and then downslope into IML-

https://doi.org/10.5194/egusphere-2026-6324
Preprint. Discussion started: 26 November 2026
© Author(s) 2026. CC BY 4.0 License.

2. There are no inflowing surface channels into IML-1, other than direct inputs from precipitation or ice melt. IML-2 (1.75 km^2 in area) is around four times larger than IML-1 and is comprised of two distinct sections with separate calving fronts (452 m and 1044 m respectively in width). The lake has a relatively large (~20 m wide) outflow channel at its southern end, enabling the routing of meltwater away from the ice margin towards Kangerlussuaq fjord via a series of connected lakes and channels (Fig. 1). NGL (0.18 km^2 in area) lies within an enclosed cirque basin and is filled with clearer, non-glacially fed water, hence resulting in a significantly lower albedo (~5%; calculated using the method of Liang, 2001) than the sediment-laden glacially fed lakes (~ 11%).

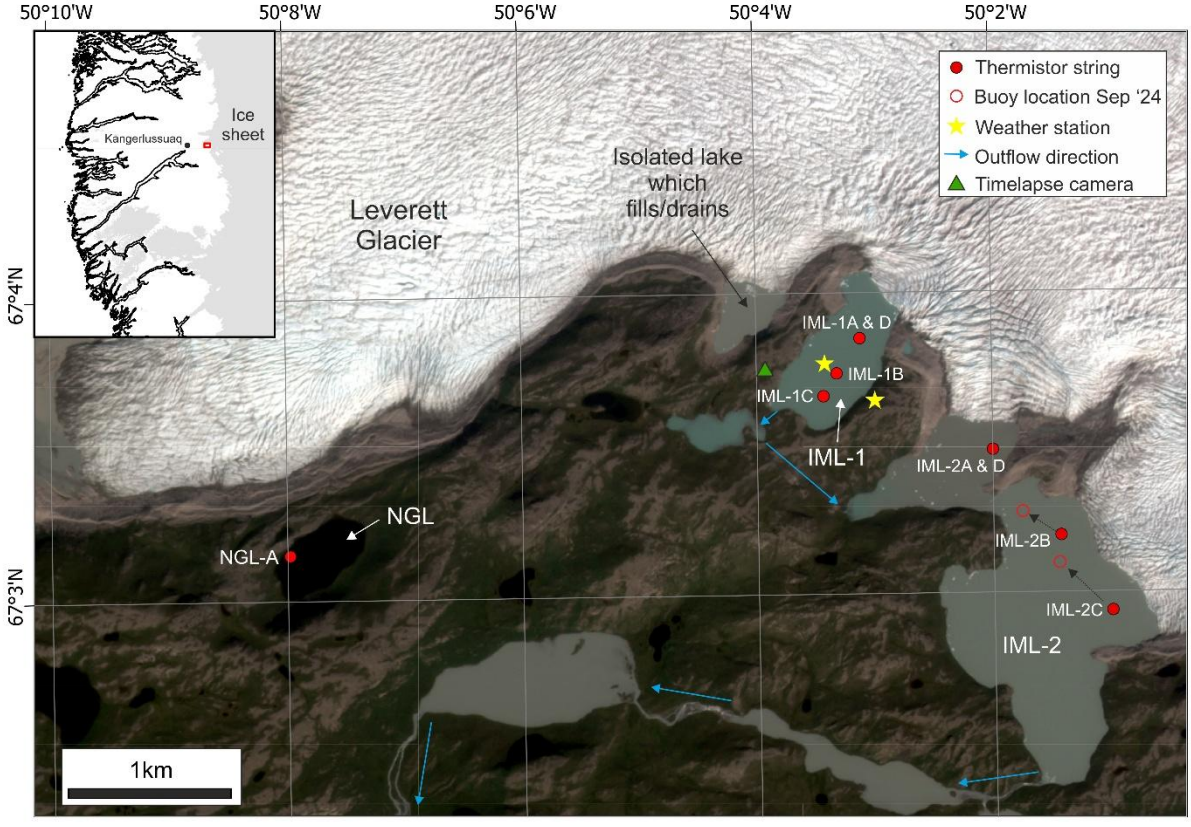


Figure 1. Study site in south-west Greenland, showing the location of the three study lakes: IML-1, IML-2 and NGL. Symbols indicate the position of thermistor strings (red circles), automatic weather stations (yellow stars) and the timelapse camera (green triangle). Movement of thermistor strings IML-2B and IML-2C between July and September 2024 is indicated by the black arrows. Blue arrows indicate the location and flow direction of connecting streams. The background is a PlanetScope SuperDove satellite image from 27/07/2024.

https://doi.org/10.5194/egusphere-2026-6324
Preprint. Discussion started: 26 November 2026
© Author(s) 2026. CC BY 4.0 License.

3 Methods

Field data were collected across three field seasons in June/July 2024, late September 2024 and July/August 2025 (Fig. 2). Lake temperature, meteorological and timelapse camera data were obtained via continuous long-term sensor deployments between June 2024 and August 2025, whilst bathymetric mapping and turbidity profiles were conducted during field seasons. A summary of the different datasets generated within this study is shown in Fig. 2.

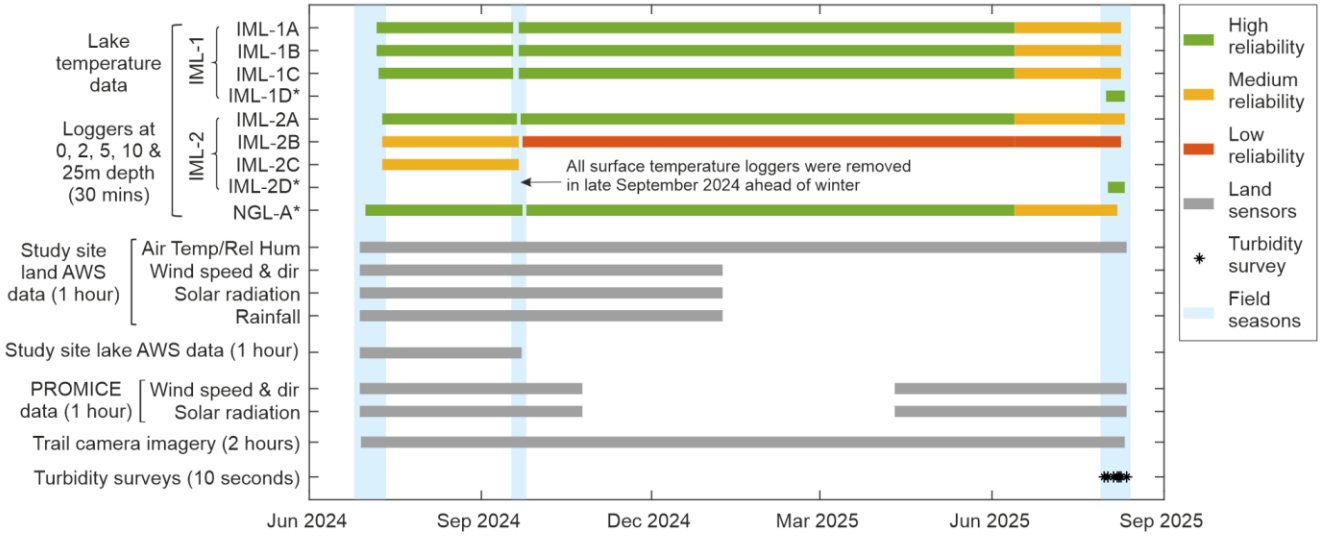


Figure 2. Summary of field datasets generated in this study, highlighting time series length and overlap between different datasets. Classifications of lake temperature data reliability are estimates only (see Section 3.4.1). Asterisks indicate thermistor strings with differing sensor spacing to the depths listed in the figure (see Section 3.4).

3.1 Meteorological observations

A land-based automated weather station (AWS), equipped with Cambell Scientific meteorological sensors, was installed between IML-1 and IML-2 (Fig. 1; 551 m asl) to monitor hourly air temperature, relative humidity, wind speed and direction, solar radiation, and rainfall. All sensors except the rain gauge (1 m height) were positioned 2 m above the ground. All land-based meteorological sensors collected data from installation on 27 June 2024 until 8 January 2025 (Fig. 2). Air temperature and relative humidity data were recorded through to September 2025. Data for wind speed and direction, solar radiation and rainfall were not collected from 9 January 2025 onwards due to animal interference with sensor cabling (Fig. 2). As a result of these data gaps, we supplemented our land-based weather station data with measurements from a PROMICE weather station (KAN-B; Fausto et al., 2026), located around 8 km north our study site. A comparison of the two datasets is shown in Supplementary Figure 1.

https://doi.org/10.5194/egusphere-2026-6324
Preprint. Discussion started: 26 November 2026
© Author(s) 2026. CC BY 4.0 License.

A second AWS was installed on a floating platform in the centre of IML-1 between July and September 2024 to provide on-lake meteorological measurements to complement our land-based data. A Campbell MetSens500 sensor measured hourly air temperature, relative humidity, wind speed and direction and barometric pressure. Lake-based meteorological measurements were recorded between 7 July – 7 September 2024, before a power issue prevented further data collection. The lake-based weather station was removed prior to winter due to logistical and power constraints.

3.2 Time-lapse camera imagery

An Acorn 6630MC 14 Megapixel time-lapse camera was installed on the south-west margin of IML-1 to capture lake surface and weather conditions. The camera was positioned to provide an oblique viewing angle with a wide field of view encompassing the majority of the lake surface. Repeat images were captured every hour between July 2024 and late September 2024, and every two hours from 03:00 – 23:00 between late September 2024 and August 2025. For the purposes of this study, camera images were used exclusively to provide context for observed fluctuations in lake temperature, and we do not provide quantitative measurements of calving activity. Imagery captured at IML-1 is assumed to be broadly representative of conditions across our study lakes, although PlanetScope SuperDove satellite imagery (available at near-daily frequency) were additionally used to constrain the timing of lake freezing/thawing of IML-2 and NGL.

Timelapse images were used to derive a daily quantitative index of lake surface conditions throughout the study period. This classification was conducted to account for the significant influence of surface ice and snow cover on lake thermal dynamics (Ellis et al., 1991). Each day was assigned a value (1-6) based on visual assessment of the imagery, representing six distinct surface states (Supplementary Fig. 2): 1) open water; 2) partially frozen; 3) frozen with surface slush or melt ponds; 4) frozen with minimal or no snow cover; 5) frozen with predominantly snow cover; 6) frozen with complete snow cover. In instances where multiple surface condition states were identified within the same day, the most common state was used. Days were assigned 'state 6' in rare instances when fresh snow accumulation obscured the lens during periods when the lake was known to be frozen.

3.3 Lake depth measurements

Bathymetry data were collected in July 2024 using a Deeper CHIRP+ 2 smart sonar (15 Hz scanning frequency), towed behind an inflatable kayak (Supplementary Figure 11). Horizontal coordinates were recorded by an internal GPS within the sensor. The sonar has a range of 15 cm – 100 m, and our accuracy assessment (conducted by comparing crossover errors at overlapping transect points) found a route mean square error of ±2.4 m. The maximum recorded depth at IML-1 was 45.8 m, 52.5 m at IML-2, and 24.4 m at NGL (Fig. 3). Spatially complete bathymetry measurements at IML-1 and NGL indicate approximate lake volumes of 7.2 x 10^6 m^3 and 2.8 x 10^6 m^3 respectively.

https://doi.org/10.5194/egusphere-2026-6324
Preprint. Discussion started: 26 November 2026
© Author(s) 2026. CC BY 4.0 License.

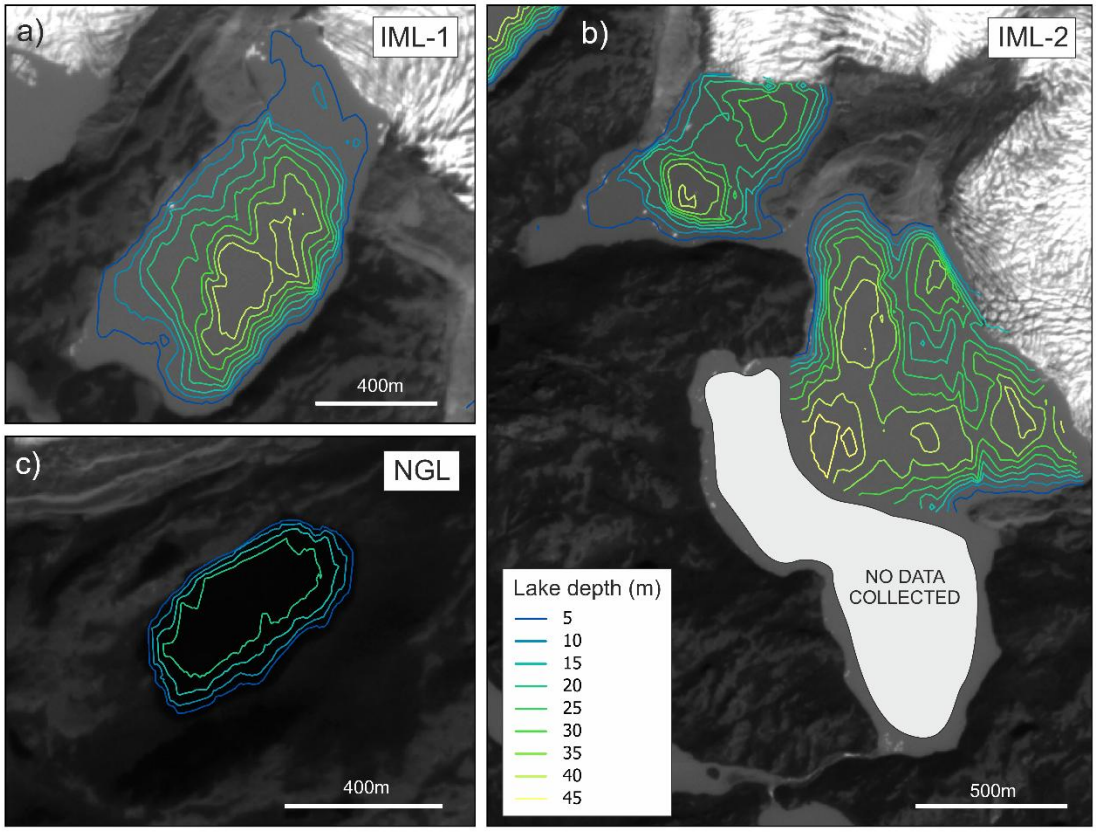


Figure 3. Lake bathymetry of IML-1 (a), IML-2 (b) and NGL (c), as recorded in July 2024.

3.4 Lake temperature measurements

Lake temperature measurements were recorded using HOBO TidBit MX2203 temperature loggers. The loggers have a manufacturer reported accuracy of ±0.2 °C, and function to a maximum depth of 120 m. Our own comparison test between loggers found a mean standard deviation of 0.04 °C, which we deem to be a more appropriate uncertainty measure when considering relative variability between sensors. Loggers were vertically distributed along lengths of static rope, hereafter referred to as thermistor strings. Temperature sensors were placed at the surface (~20 cm depth, due to the buoy partially sitting underwater), 2 m, 5 m and 10 m on each thermistor string. The uppermost part of the water column is where the greatest variability in temperature would be expected, and our spacing follows the approach of similar lake temperature studies (Scoffield et al., 2025). Sensors were additionally placed at 25 m and 40 m for strings where the water depth exceeded these values. Each thermistor string was anchored at the lake bed with a sandbag and held vertically within the water column by a surface buoy. Loggers measured water temperature every 10 minutes, recording the average value every half hour.

https://doi.org/10.5194/egusphere-2026-6324
Preprint. Discussion started: 26 November 2026
© Author(s) 2026. CC BY 4.0 License.

Seven thermistor strings, comprising 37 temperature loggers in total, were deployed across the three study lakes in early July 2024. Strings were deployed as soon as possible after the thawing of surface ice from each respective lake; this occurred on approximately 25 June (NGL), 6 July (IML-1), and 7 July (IML-2). Three thermistor strings were installed in IML-1 at distances of ~300 m (IML-1A), ~550 m (IML-1B) & ~750 m (IML-1C) from the ice margin (Fig. 1), to investigate potential temperature variability with ice margin proximity. The wider geometry and longer ice-lake interface of IML-2 made it more suited for investigating potential lateral variability in lake temperatures across the ice margin. Thermistor strings in IML-2 were therefore positioned at roughly equal distances from the ice front (between 150 – 250 m); one in front of the shorter calving front (IML-2A), and two on opposite sides of the longer calving front (IML-2B and IML-2C; Fig. 1). Thermistor strings were placed at this distance from the ice margin as it offered the greatest average depth across the lake width, thus maximising the depth from which temperature data could be collected. A single additional thermistor string (NGL-A) was deployed at approximately the deepest point of NGL. Additional thermistor strings were not considered necessary because non-glacial lakes are less likely to have lateral or longitudinal temperature variability than ice-marginal lakes.

Thermistor strings were temporarily lifted, shortened by two metres, and redeployed in September 2024 to avoid being crushed or caught in lake surface ice over winter months. During this redeployment, surface buoys and sensors were removed, with smaller sub-surface buoys installed at 2 m depth to keep strings vertical and taught, whilst avoiding the risk of being punctured by ice. Thermistor string IML-2C was not redeployed following removal in September 2024 due to experiencing significant horizontal (~300 m) and vertical movement of sensors.

Two additional thermistor strings (IML-1D & IML-2D) were installed for ~10 days in IML-1 and IML-2 respectively during the 2025 field season for two primary reasons: 1) The break-up of lake-surface ice in June 2025 dragged some of the long-term thermistor strings to shallower depths, introducing uncertainty regarding the exact depth of temperature loggers. 2) Preliminary results from the 2024 lake temperature data indicated potential differences in subglacial meltwater supply between IML-1 & IML-2. Additional higher-spatial resolution strings were hence required to enable us to compare the thermal structure of the lakes in greater detail. Eleven temperature loggers were placed every three metres along the length of both new strings. Strings IML-1D and IML-2D were placed at approximately the same positions as IML-1A and IML-2A.

3.4.1 Sensor performance and reliability

Lake temperature data were recovered from all seven long-term thermistor string moorings. A total of 37 out of 42 temperature loggers recorded data successfully for the duration of their deployment. Five loggers experienced water ingress, resulting in incomplete time series for part or the entirety of the study period; no data were recovered from sensors IML-1B-25 (Ice-marginal lake 1, thermistor string 1B, 25 m depth logger), IML-1B-40, or NGL-20 between June-September 2024, and from sensors IML-1B-5, IML-1B-40 or NGL-A-5 between September 2024 – August 2025. The two short-term thermistor strings deployed for ~10 days in August 2025 collected data throughout (IML-1D & IML-2D).

https://doi.org/10.5194/egusphere-2026-6324
Preprint. Discussion started: 26 November 2026
© Author(s) 2026. CC BY 4.0 License.

Underwater temperature loggers attached to long-term moorings are inherently susceptible to minor changes in spatial location (Kirchner et al., 2024), introducing potential uncertainty in our lake temperature data. To ensure analytical rigor, we categorised our thermistor string data as 'high', 'medium' or 'low' reliability (Fig. 2) and focussed our analysis on the highest reliability data. Data were classified as 'high reliability' where thermistor string locations exhibited strong spatial stability (< 50 m), vertical temperature profiles were coherent, and seasonal trends were consistent across adjacent sensors. Data associated with thermistor string movement, such as from iceberg interference or following ice-breakup in June 2025, were classed as 'medium' reliability. Although subject to some positional uncertainty, strong thermal coherence across strings suggests that relative trends and thermal variability between sensors can be interpreted with confidence. Data from thermistor string IML-2B were classed as 'low' reliability from September 2024 onwards due to displaying erratic and implausible data throughout the entire winter period (Fig. 2). Comparisons between lake temperatures in IML-1 and other study lakes are hereafter focused on data from IML-1A, as only minor variability was recorded between thermistor strings IML-1A, IML-1B & IML-1C (Supplementary Fig. 3). All three strings conformed to the same seasonal trends, vertical temperature distributions and stratification timings and characteristics throughout the study period. Full time series for all seven strings are provided in the Supplement (Supplementary Figs. 4-10).

3.5 Turbidity measurements

To investigate potential variability in subglacial meltwater input between study lakes, transient turbidity profiles were obtained using a RBR*solo*^{3} turbidity probe during the 2025 field season (Fig. 2). Singular profiles were acquired at thermistor strings IML-2B and NGL-A, with repeat profiling conducted at thermistor strings IML-1D (n = 5) and IML-2D (n = 4). These repeat profiles were distributed across varying times of day, meteorological conditions, and suspected melt intensities to capture potential variability in subglacial meltwater input. All profiles were conducted between 31 July and 12 August 2025 (Supplementary Table 1). Measurements were recorded at 3 m intervals throughout the water column, aligning with the depths of temperature loggers on thermistor strings IML-1D and IML-2D. At each depth, turbidity was logged every ten seconds for two minutes; the resulting values were averaged to provide a mean value per depth for analysis.

3.6 Statistical correlation analysis

Thermistor string lake temperature data were correlated against land-based air temperature and solar radiation data to investigate the broad-scale influence of atmospheric effects on lake temperature. Analyses were based on 71 days of data from summer 2024, spanning 10 July – 18 September (the period of overlapping data collection prior to removal of lake surface thermistors). Mean daily values were used to eradicate the influence of diurnal signals within the data. The Pearson correlation coefficient was calculated for each individual thermistor, enabling comparison between different lakes, thermistor strings, and lake depths.

https://doi.org/10.5194/egusphere-2026-6324
Preprint. Discussion started: 26 November 2026
© Author(s) 2026. CC BY 4.0 License.

4 Results

4.1 Meteorological conditions

Hourly land-based air temperatures ranged from -27.3 to 13.5 °C during our study period. During July and August 2024, mean daily air temperatures were typically between 1 and 10 °C (Fig. 4), with a mean diurnal range of ~5 °C. Daily minimum air temperatures regularly dropped below freezing from early September 2024, with daily mean temperatures consistently below 0 °C from 7 October 2024. The 2024/25 extended winter period (November – April) was characterised by fluctuating, quasi-monthly synoptic time-scale variability in air temperature, ranging from -27.3 °C to +7.2 °C. These cycles included several rapid warming and cooling events, often with changes of 15-25 °C within just a few days (Fig. 4); the most rapid increase occurred between 8 and 9 March 2025, when air temperature rose from -20.1 °C to +4.3 °C within 27 hours. Distinct winter 'warm' periods with positive daily mean air temperatures were recorded between 12 and 13 February, 9 and 13 March, 8 and 9 April and 15 and 20 May (Fig. 4). Mean daily temperatures were consistently above 0 °C from late-May 2025 through to August 2025. On-lake air temperatures during summer 2024 largely mirrored land-based diurnal and seasonal patterns, although peak daily temperatures were typically 1-2 °C cooler than on land (Supplementary Fig. 12).

Maximum daily peaks in solar radiation reached 700-800 W/m^2 in June 2024 and June 2025, dropping to <10 W/m^2 in mid-December 2024 (Supplementary Fig. 13). Daylight varied from 24-hours in mid-summer to 1.5 hours in mid-winter. Mean daily solar radiation ranged from ~0.1 W/m^2 to ~420 W/m^2 (Fig. 4). Mean daily land-based wind speeds typically ranged between 1 and 8 m/s, although wind speeds exceeding 10 m/s occasionally persisted for several hours (Supplementary Fig. 14). The maximum recorded land-based wind speed was 24.7 m/s, in early December 2024, although no wind data were recorded after mid-January 2025 due to sensor failure. No clear seasonal trends in wind speed were recorded, either in our data or PROMICE data (Supplementary Fig. 14). Winds recorded at our land-based AWS had a clear prevailing direction; 80% of wind measurements (July 2024 – January 2025) came from an easterly to south-south-easterly direction. Lake-based wind speeds broadly mirrored land-based measurements, exhibiting no systematic offset in variability (Supplementary Fig. 15).

4.2 Lake surface conditions

Lake surface conditions were assessed from trail camera imagery for IML-1, and remotely from PlanetScope optical satellite data for all lakes. Following winter 2023/24 ice cover, the lakes became completely free of surface ice on 25 June 2024 (NGL), 6 July (IML-1) and 7 July (IML-2). All three lakes subsequently experienced open water conditions for ~3.5 months through to early October 2024, before starting to freeze-over. Satellite data show complete ice cover on all lakes by 16 October 2024. Ice cover over the 2024/25 winter period persisted until June 2025 (~75% of the year; Fig. 4), with complete ice-off observed on 16 June (NGL), 22 June (IML-1) and 23 June (IML-2) respectively. Transitional periods of lake freezing and thawing, characterised by partially frozen lake surfaces, lasted between one and three weeks across the study lakes.

https://doi.org/10.5194/egusphere-2026-6324
Preprint. Discussion started: 26 November 2026
© Author(s) 2026. CC BY 4.0 License.

All lakes experienced variable snow-cover whilst frozen between mid-October 2024 and mid-June 2025. Whilst timelapse images were not captured at IML-2 and NGL, timings of lake-ice snow cover and snowmelt events are assumed to be broadly similar to those observed at IML-1. Following an initial period of ice-cover with no snow cover, IML-1 was continuously snow-covered between 4 November 2024 and 12 February 2025 (Fig. 4). From mid-February to mid-May, periods of continuous lake snow cover were interspersed with short-lived snowmelt events, coinciding with positive air temperatures. These transient warm periods (Section 4.1) caused snowmelt at the lake surface, resulting in the formation of surface slush and liquid melt ponds on an exposed lake-ice surface. The last day of lake-ice snow cover from the winter period was on 14 May; following this date, the lake surface was either characterised by bare ice or slush/water-covered ice. The first images of open-water around the edge of IML-1 were recorded on 21 May, whilst the widespread break-up of lake-surface ice started on ~13 June 2025.

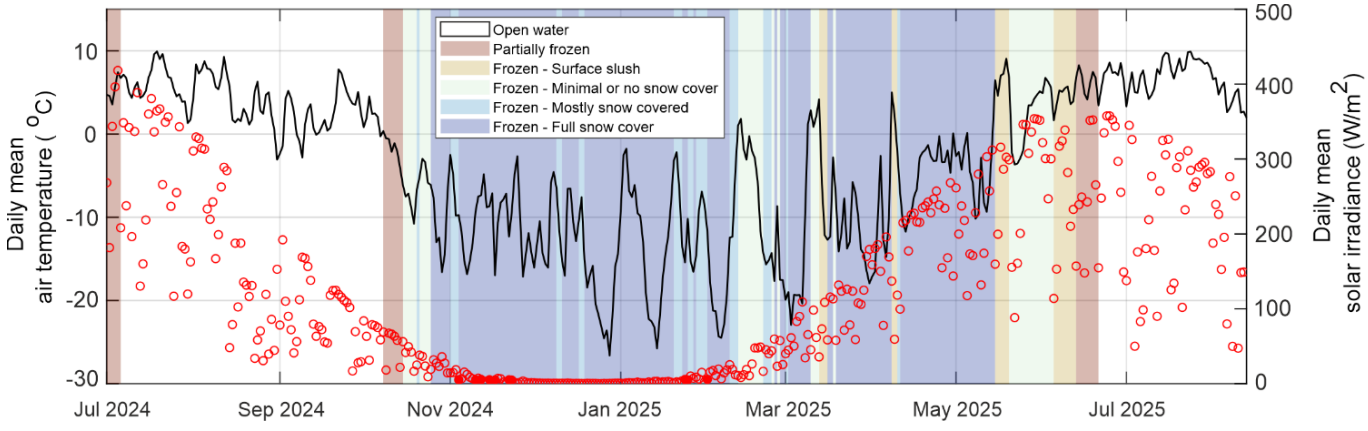


Figure 4. Air temperature (black), solar radiation (red circles) and lake surface conditions (vertical coloured patches) throughout the study period. The surface conditions displayed here are based on timelapse camera observations from IML-1, but are assumed to be broadly representative of conditions at all study lakes. The black line displays mean daily averaged air temperature from the land-based AWS, whilst red circles show mean daily solar radiation from the PROMICE weather station (see Methods). Example images for each lake surface state are shown in Supplementary Figure 2.

4.3 Lake temperature

We describe lake temperature observations across five distinct time periods throughout our study timeframe, defined by sensor deployment windows and key seasonal transitions: (i) Summer 2024 (10 July – 17 September 2024), constrained by thermistor string deployment and recovery during open-water conditions; (ii) 2024 freezing period (1 – 31 October 2024), defined by autumn water column cooling and surface ice cover formation; (iii) 2024/25 winter ice cover (1 November 2024 – 14 May 2025), defined by consolidated surface ice cover and relatively stable under-ice thermal conditions; (iv) 2025 thawing period

https://doi.org/10.5194/egusphere-2026-6324
Preprint. Discussion started: 26 November 2026
© Author(s) 2026. CC BY 4.0 License.

(15 May – 23 June 2025), defined by progressive surface ice thawing and heightened lake thermal sensitivity to atmospheric forcing; and (v) Summer 2025 (1 – 11 August 2025), constrained by the operational window of thermistor strings IML-1D and IML-2D.

4.3.1 Summer 2024

NGL was the warmest lake during summer 2024 (10 July–18 September; Fig. 5), with surface temperatures ranging from 5.16 to 13.00 °C (median 9.41 °C; Fig. 6). Median temperatures were only marginally cooler at 2 m (9.35 °C) and 5 m (9.23 °C) depth, whilst the 10 m level was ~1 °C cooler on average. At the start of observations (1–6 July 2024), NGL was already stratified, with a warm, low-density surface layer overlying cooler, denser deep water (Fig. 5a). On 7 July, a transient wind event induced mixing that disrupted stratification, temporarily making the lake isothermal. Between 8 and 23 July, an extended period of calm conditions enabled the re-establishment of stratification, characterised by rapid surface warming above a thermally stable 10 m layer (Fig. 5a). Two major surface warming peaks occurred following prolonged (>7 days) periods of high solar radiation, warm air temperatures, and low wind speeds (Fig. 4): a seasonal maximum peak on 23 July (13.00 °C) and a secondary peak on 10 August (11.93 °C; Fig. 5a). From mid-August onward, declining solar irradiance limited the lake's capacity to re-stratify following a wind-driven mixing event on 11 August. Surface cooling and downward convection subsequently maintained isothermal conditions throughout the seasonal cooling phase, disrupted only by minor diurnal fluctuations at the lake surface.

IML-1 mirrored the timing of several thermal shifts at NGL in response to shared atmospheric forcing, but differed in absolute water temperatures and vertical structure. IML-1 was significantly colder than NGL at all depths; the median surface temperature at IML-1A was 5.39 °C, decreasing progressively with depth to 4.57 °C at 25 m (Fig. 6). At the start of the observational period (7 July), the lake was isothermal with water temperatures below 4 °C. This difference with NGL was likely driven by lower solar radiation absorption due to higher surface albedo, a cooling effect from glacial meltwater input, and delayed winter ice breakup. Once the water column warmed past the ~4 °C maximum density threshold in mid-July, positive thermal stratification established. Water temperatures remained above 4 °C at all depths through to mid-September (Fig. 5b), maintaining stratification. The only major breakdown in stratification occurred in late July, when multi-day wind events induced full-depth mixing. Surface temperatures exceeded 6 °C for approximately four weeks across the summer period and mirrored NGL's warming peaks on 22–23 July and 10 August. However, unlike NGL, subsurface waters (2 m and 5 m) remained markedly cooler during these surface warming events; on 22 July, for example, peak surface temperature reached 9.05 °C, whereas maximum temperatures at 2 m and 5 m reached only 6.88 °C and 5.48 °C respectively (Fig. 5b).

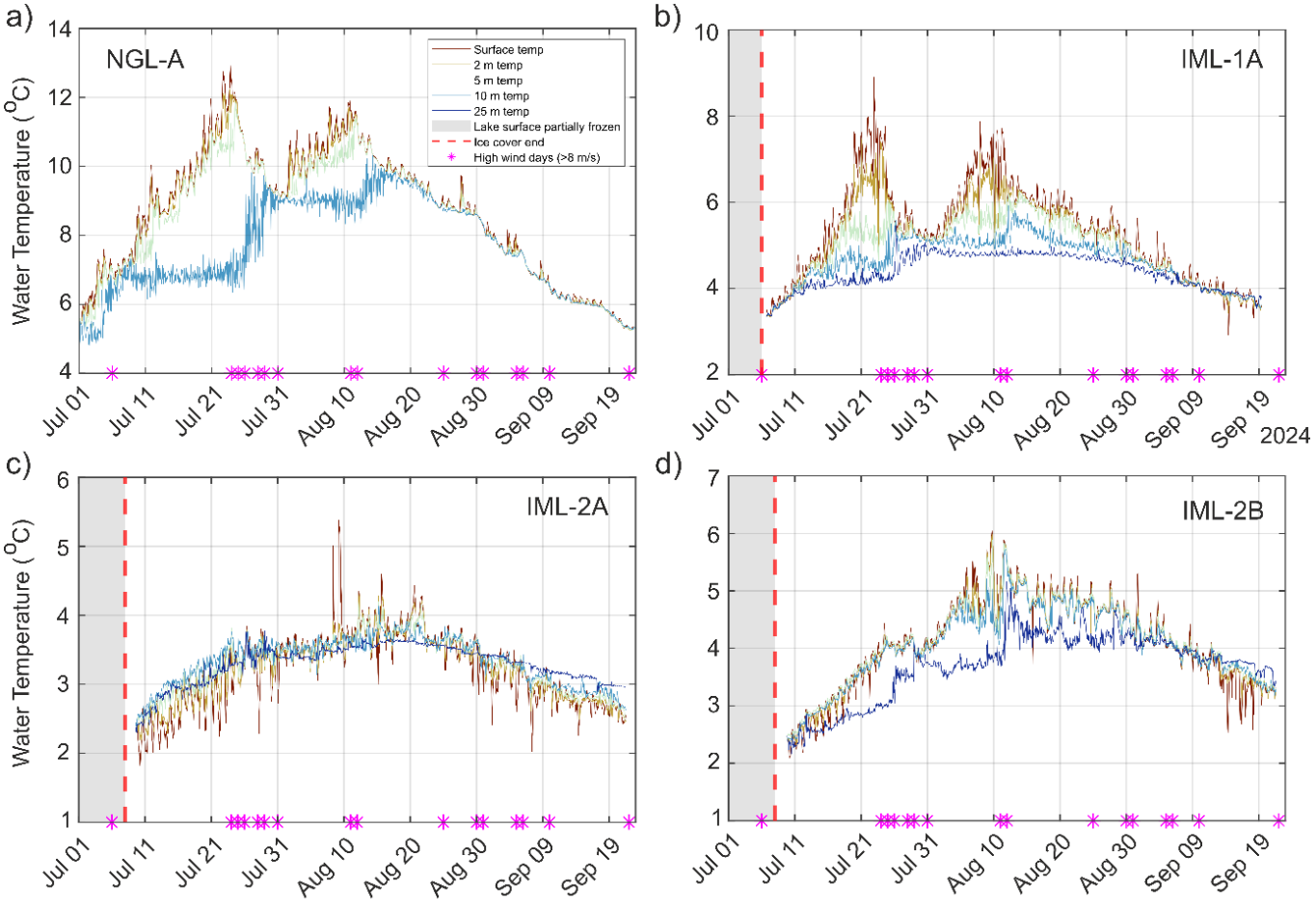
The two basins of IML-2 (Fig. 1) displayed differing thermal characteristics. IML-2B (located adjacent to the larger calving front) exhibited seasonal warming and cooling trends similar to NGL and IML-1A, but with reduced stratification strength due to cooler overall surface temperatures (Fig. 5d). Surface temperatures remained below 4 °C throughout July, keeping the water column largely isothermal and inhibiting stable thermal stratification. Stratification established in early August once surface

https://doi.org/10.5194/egusphere-2026-6324
Preprint. Discussion started: 26 November 2026
© Author(s) 2026. CC BY 4.0 License.

temperatures climbed above approximately 4 °C, resulting in higher surface temperatures in August than in July and a peak surface temperature of 6.01 °C on 9 August (Fig. 5d). Deep water at IML-2B (25 m depth) displayed pronounced seasonality, shifting from the coldest portion of the water column in July and August to the warmest by mid-September.

IML-2A (located adjacent to the smaller calving front) departed most significantly from the 'control' thermal dynamics observed at NGL. Temperatures remained below 4 °C at all depths throughout summer 2024, except for brief surface warming spikes in mid-August (Fig. 5c). Consequently, IML-2A maintained an inverse thermal regime for much of the season, with median temperatures increasing with depth from the surface (3.34 °C) to 10 m (3.46 °C; Fig. 6). The only exception to this inverse regime occurred during the first three weeks of August, when surface warming temporarily inverted this gradient. The 25 m layer at IML-2A displayed clear dynamic seasonal shifts across the summer period, as similarly observed at IML-2B. IML-2A-25 was warmer than the surface but cooler than 10 m in July, became the coldest layer in August, and transitioned to the warmest layer from September onward (Fig. 5c). This configuration disrupted the thermal structure that would be expected if the stability of the lake were solely controlled by temperature-driven density variation, suggesting additional influences from glacial sediment.

https://doi.org/10.5194/egusphere-2026-6324
Preprint. Discussion started: 26 November 2026
© Author(s) 2026. CC BY 4.0 License.



335 **Figure 5.** Lake temperature time series for thermistor strings NGL-A (a), IML-1A (b), IML-2A (c) and IML-2B (d) between July and September 2024, displaying hourly lake temeprature at varying depths. No data are displayed for 20 m depth at NGL-A (a) due to a sensor failure.

https://doi.org/10.5194/egusphere-2026-6324
Preprint. Discussion started: 26 November 2026
© Author(s) 2026. CC BY 4.0 License.

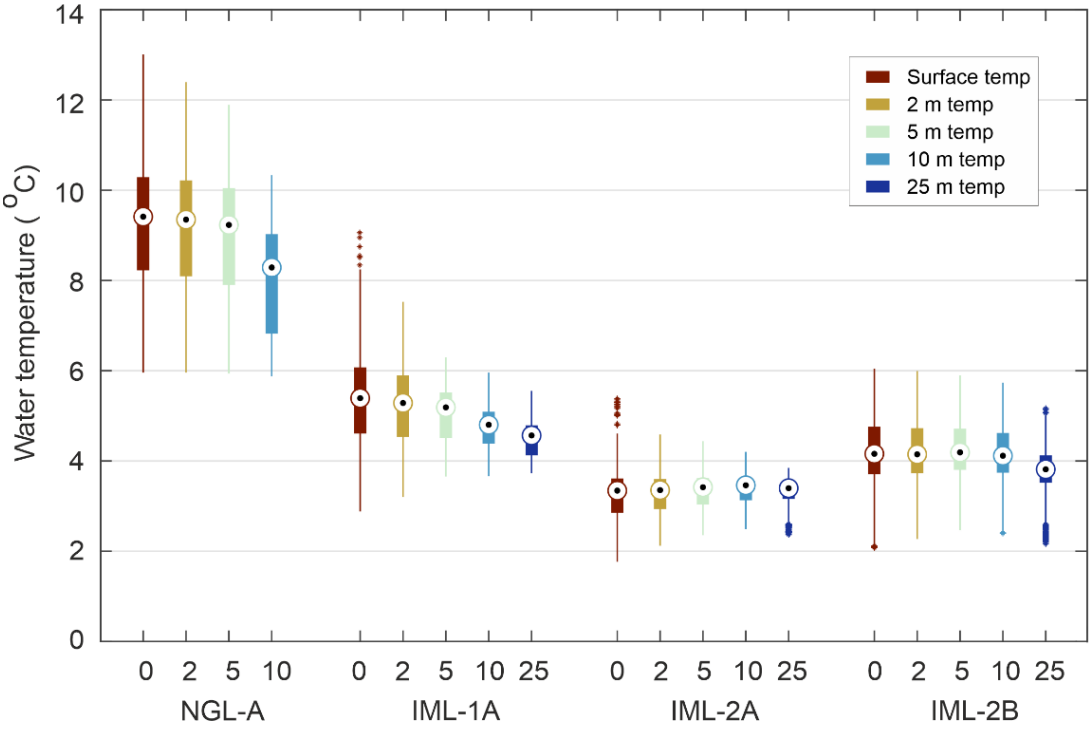


Figure 6. Boxplots of lake temperature distribution for thermistor strings NGL-A, IML-1A, IML-2A and IML-2B and during summer 2024. All results are based on temeprature data collected between 10 July – 17 September 2024. Boxplots show the median (black dots), interquartile ranges (box ends indicate the 25th and 75th percentiles), and the range of data (whiskers) when excluding outliers (greater than 1.5 times the interquartile range), which are plotted as individual asterisks.

4.3.2 2024 freezing period

The freezing period for all three lakes occurred during October 2024, driven by declining air temperatures through late September and early October (Fig. 4). Night-time air temperatures consistently dropped below freezing from 1 October onwards, whilst daily maximum air temperatures did not exceed 0 °C from 13 October onwards. Throughout this period, the thermal structure of all three lakes transitioned from near-isothermal to cryostratified (inversely stratified beneath surface ice; Yang et al., 2021), characterised by the separation of depth-dependent lake temperatures. However, the timing and nature of this transition differed between the lakes. NGL remained isothermal until 11 October, when lake temperatures were ~3.2 °C at all depths (Fig. 7a). Over the following week, coinciding with progressive lake surface freezing, lake temperatures stabilized in reverse depth order. Near-surface waters continued to cool the longest and at the fastest rate. Winter stability occurred on ~11 October at 20 m depth, ~16 October at 10 m depth and ~17 October at 2 m depth (Fig. 7a). NGL-A-2m recorded a

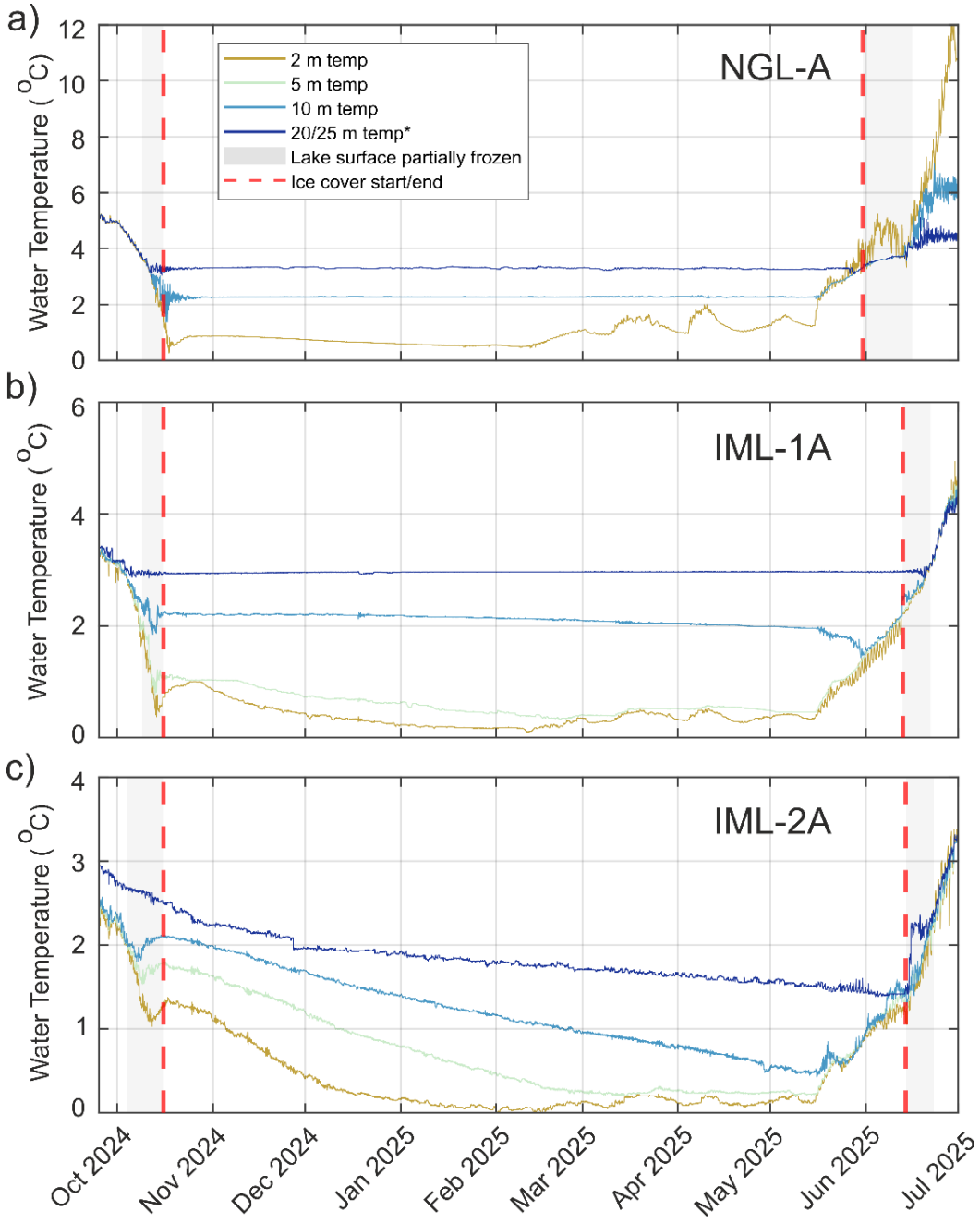
https://doi.org/10.5194/egusphere-2026-6324
Preprint. Discussion started: 26 November 2026
© Author(s) 2026. CC BY 4.0 License.

minimum temperature of 0.23 °C on the 17 October, representing the coldest temperature recorded across the entire study period within NGL. Fluctuations and minor increases (~0.6 °C) in lake temperature were subsequently observed following complete surface ice-cover.

IML-1 displayed depth-dependent separations in water temperature and absolute temperature values similar to those recorded at NGL. However, this transition started around 10 days earlier than for NGL. The deepest water (IML-1A-25m) stabilised at ~3.1 °C on ~1 October, whilst water above continued to cool (Fig. 7b). Between 1 – 13 October, water at 2 m depth cooled by ~2.8 °C to a minimum of 0.3 °C, whilst water at 10 m depth cooled more slowly, dropping by ~1.3 °C over the same period. As observed at NGL, the formation of lake-wide surface ice cover halted further lake temperature declines, with a subsequent temperature increase of ~0.7 °C recorded at IML-1A-2m between 17 – 25 October (Fig. 7b).

IML-2 differed in thermal characteristics during the ice-on period because the lake was not fully isothermal prior to freezing and temperatures remained variable. Whilst the upper layers of the lake were relatively well mixed in late September 2024 at around 2.3 °C, water at 25 m depth was approximately 0.5 °C warmer (Fig. 7c). IML-2-25 displayed a continuous, gradual temperature decrease throughout the ice-on period, contrasting with the abrupt stagnations observed at depth in IML-1 and NGL. Nearer the lake surface, water between 2 – 10 m depth cooled during early October, but at a slower rate and to a less extreme minimum than recorded at IML-1. Between 1 – 13 October, water at 2 m depth cooled from 2.2 °C to 1.0 °C, which was less than half the temperature change observed over the same time period at IML-1A. Consequently, despite IML-2 being considerably colder than at IML-1 and NGL throughout the summer months, its lake temperatures at the point of complete ice-on were equivalent to or slightly warmer than those of the other study lakes.

https://doi.org/10.5194/egusphere-2026-6324
Preprint. Discussion started: 26 November 2026
© Author(s) 2026. CC BY 4.0 License.



375

Figure 7. Lake temperature time series for thermistor strings NGL-A (a), IML-1A (b) and IML-2A (c) between 25 September 2024 (following the removal of surface loggers in mid-September 2024) and 1 July 2025. Dark blue lines represent 25 m depth for IML-1A and IML-2A, and 20 m depth for NGL-A. No data are displayed for 5 m depth at NGL-A due to a sensor failure.

https://doi.org/10.5194/egusphere-2026-6324
Preprint. Discussion started: 26 November 2026
© Author(s) 2026. CC BY 4.0 License.

4.3.3 2024/25 winter ice cover

NGL and IML-1 displayed highly similar thermal structures and absolute water temperatures throughout the winter ice cover period (defined here as 1 November – 14 May; section 4.3). Both lakes recorded stable, consistent temperatures at depth (Fig. 7a & b); NGL had mean water temperatures of 2.3 °C (SD = <0.01 °C) and 3.3 °C (SD = 0.02 °C) at 10 m and 20 m depth respectively, whilst IML-1 had mean temperatures of 2.1 °C (SD = 0.02 °C) and 3.0 °C (SD = 0.01 °C) at 10 m and 25 m depth. By contrast, lake temperatures at depth in IML-2A displayed a continuous decreasing trend throughout winter, with notably greater hourly-to-daily variability (Fig. 7c). Between 1 November and 14 May, water temperature at IML-2A-25m decreased from ~2.3 °C to 1.5 °C, while the temperature at IML-2A-10m decreased from 2.0 °C to 0.5 °C. The standard deviation of detrended lake temperatures during this period was 0.04 °C (10 m) and 0.05 °C (25 m). Although low in absolute terms, this variability was two to six times greater than that experienced at the same depths in NGL and IML-1 (Fig. 8).

Nearer the lake surface (2 and 5 m depths), all study lakes experienced gradually decreasing water temperatures during the first three months of winter, though at varying rates. Between 1 November 2024 and 1 February 2025, the daily mean lake temperature at 2 m depth decreased by ~0.32 °C at NGL, ~0.65 °C at IML-1, and ~1.17 °C at IML-2. Similar to observations at greater depths, the variability in detrended 2 m temperatures during this three-month period was greater at IML-2 (SD = 0.11 °C) than at IML-1 (SD = 0.06 °C) or NGL (SD = 0.02 °C). Decreasing 2 m lake temperatures during this period displayed no apparent associations with changes in air temperature, solar radiation or wind speed. All lakes reached their minimum winter 2 m lake temperature between 10 and 13 February, before showing minor temperature increases during the second half of the month (Fig. 7). This warming coincided with daily mean air temperatures of 1.0 °C and 1.8 °C on 12 and 13 February respectively, marking the first positive daily air temperatures since early October 2024.

From mid-February to early May, near-surface (2 m) loggers across all three lakes recorded minor, weekly-scale water temperature fluctuations (Fig. 7), likely in response to large changes in air temperature (Fig. 4). This variability was most pronounced in NGL, where weekly changes in 2 m water temperature varied by up to 1 °C, often superimposed by a diurnal signal, especially during warming phases (Fig. 7a). More subdued weekly changes of 0.2-0.3 °C were recorded in IML-1 and IML-2, although some diurnal variability was also detected. Temperature variability was less pronounced at 5 m depth in IML-1 and IML-2 (<0.1 °C) during this period. No winter data were retrieved from NGL-A-5m.

https://doi.org/10.5194/egusphere-2026-6324
Preprint. Discussion started: 26 November 2026
© Author(s) 2026. CC BY 4.0 License.

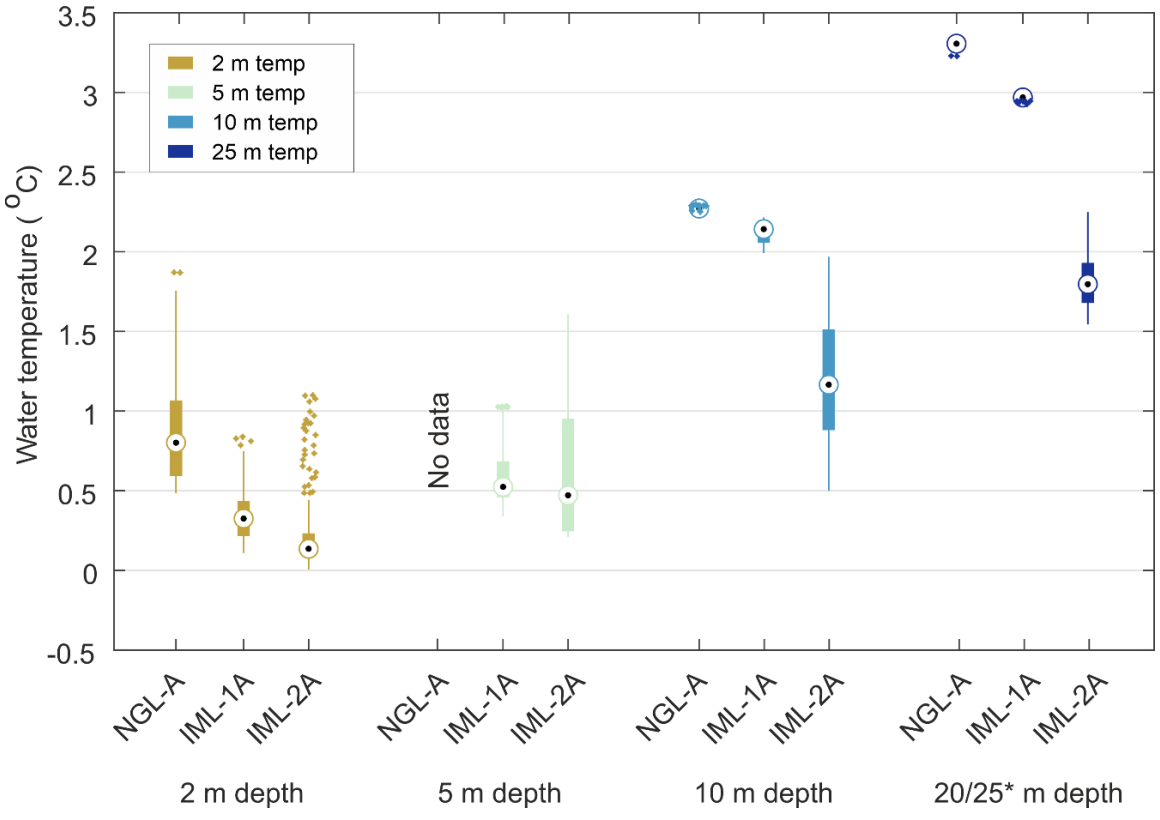


Figure 8. Boxplots of lake temperature distribution for thermistor strings NGL-A, IML-1A and IML-2A during the winter ice cover period (defined here as 1 November 2024 – 14 May 2025). Boxplots to be interpretted as described in Figure 6. Outlier points are jittered horizontally to prevent overplotting.

4.3.4 2025 thawing period

Although all three lakes remained at least partially covered by surface ice until mid- to late June 2025, they all displayed significant changes in thermal characteristics from 15 May onward (Fig. 7). Hence, the thawing period is defined here as extending from 15 May to 23 June 2025 (when all three lakes became clear of surface ice). On 15 May, water at 2, 5 and 10 m depth in all three lakes recorded sudden, rapid changes in temperature of greater magnitude and variability than any observed since October 2024 (Fig. 7). These abrupt temperature changes followed a rapid and continuous rise in air temperature from -12.4 °C at 06:00 on 12 May to 8.4 °C at midnight on 15 May (Fig. 4). This warm period melted all surface snow on IML-1 (and presumably also on IML-2 and NGL), with 14 May marking the final day of lake surface snow cover prior to the summer period (Fig. 4). At NGL, 2 m temperature increased by ~1 °C within 24 hours between 15 and 16 May, followed by a more gradual warming trend for the remainder of the month prior to lake ice breakup. A similar pattern of increasing 2 m

https://doi.org/10.5194/egusphere-2026-6324
Preprint. Discussion started: 26 November 2026
© Author(s) 2026. CC BY 4.0 License.

temperatures initiated on 15 May at IML-1 and IML-2. Between 15 May and 12 June, daily mean temperature at IML-1A-2 progressively increased from 0.3 °C to 2.0 °C, with distinct diurnal cycles varying by ~0.3 °C (Fig. 9a). These diurnal cycles ceased from 13 June onwards, despite continuing increases in daily mean water temperature. Between 13 and 21 June, the mean diurnal temperature range at IML-1A-2 was less than 0.1 °C; three times lower than in previous weeks. This shift in diurnal signal coincided with the first observations of wind-driven ice movement on the surface of IML-1 on 13 June (Fig. 9f). At IML-2A, 2 m temperature similarly gradually increased from 0.1 °C to 1.2 °C between 15 May – 12 June, prior to lake ice breakup in mid-June.

At intermediate lake depths, contrasting patterns in water temperature were observed between the three lakes from mid-May to mid-June. At NGL, water at 10 m depth began a month-long period of continuous warming on 15 May, marking the end of seven months of winter thermal stability. Winter temperature stasis similarly ended around 15 May at IML-1A-10m, but instead of warming, mean daily water temperature steadily dropped from 2.0 °C on 15 May to 1.5 °C on 31 May (Fig. 7b). This drop was immediately followed by a reversal to gradual warming through early June (~0.05 °C per day), before a sudden jump of 0.3 °C on the 13 June prior to lake ice breakup. At IML-2A, 10 m temperature began increasing on the 16 May, ending the continuous decline observed throughout the winter.

At greater depth (25 m), water temperatures did not deviate from their winter behaviour until closer to the onset of lake ice breakup. At NGL-A and IML-1A, winter thermal stasis persisted at 25 m depth until ~27 May and ~18 June respectively (Fig. 7a & b). At IML-2A-25, the gradual winter temperature decline ended around 14 June, when 25 m water temperature rapidly increased from 1.4 °C to 2.3 °C over a 24-hour period. Across all lakes, temperature changes at 25 m occurred once the overlying waters had warmed sufficiently to match the temperature at depth, thereby ending winter cryostratification. Following the completion of lake ice breakup, IML-1 and IML-2 continued to warm isothermally through late June 2025, whilst NGL established a stratified structure (Fig. 7).

https://doi.org/10.5194/egusphere-2026-6324
Preprint. Discussion started: 26 November 2026
© Author(s) 2026. CC BY 4.0 License.

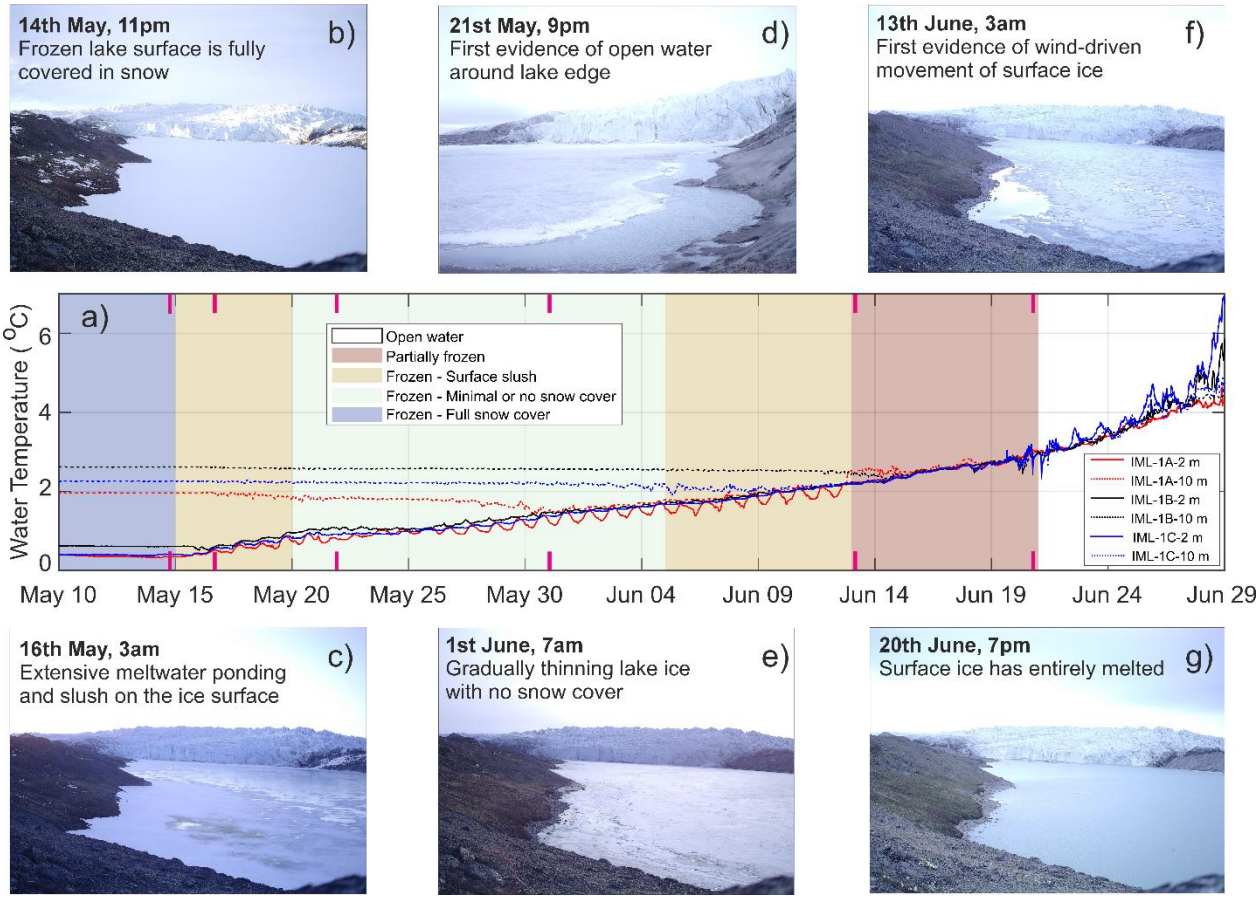


Figure 9. (a) Lake temperature time series for IML-1 between mid-May and mid-June 2025, here referred to as the thawing period (Section 4.1.4). Lake temepratures are displayed at 2 m (solid lines) and 10 m (dotted lines) lake depth for IML-1A (red), IML-1B (black) and IML-1C (blue). Background vertical colour bars indicates lake surface condition, as shown in Figure 2. Pink ticks indicate the dates of trail camera images shown in (b-g). (b-g) Trail camera images of IML-1 at key stages during the thawing period.

4.3.5 Summer 2025

Lake temperature data during summer 2025 were acquired from thermistor strings IML-1D and IML-2D for ~10 days betweeen 1 and 11 August 2025 (see Section 3.4). Warmer lake temperatures were recorded at IML-1D than at IML-2D at all depths, consistent with IML-1 being the warmer lake during summer 2024 (Figs. 5 & 6). Water temperatures at IML-1D ranged from a maximum of 8.75 °C at the surface to a minimum of 4.27 °C at 30 m depth, maintaining a typical summer stratification vertical structure of declining temperatures with depth throughout the entire 10-day period (Fig. 10a). Stratification on both

https://doi.org/10.5194/egusphere-2026-6324
Preprint. Discussion started: 26 November 2026
© Author(s) 2026. CC BY 4.0 License.

lakes between 1 – 5 August was disrupted by a wind-driven mixing event on 6 August, which thereafter limited surface temperatures.

Although lake temperatures at IML-2D were cooler than at IML-1D, they were slightly warmer than those recorded at IML-2 during summer 2024; a maximum surface temperature of 6.53 °C was recorded on 3 August, which was more than 1 °C warmer than any temperature recorded in IML-2 in 2024. A regular stratification structure was observed at IML-2D between 1 – 8 August. However, on 9 August, a notable and sharp increase in temperature occurred at depth, with all loggers below 21m recording a temperature increase of around 0.25 °C (Fig. 10b), disrupting the ordered thermal structure. Between 9 and 12 August, the coldest waters at IML-2D were at intermediate depths (12-18 m), with warmer water persisting both at depth and at the surface.

https://doi.org/10.5194/egusphere-2026-6324
Preprint. Discussion started: 26 November 2026
© Author(s) 2026. CC BY 4.0 License.

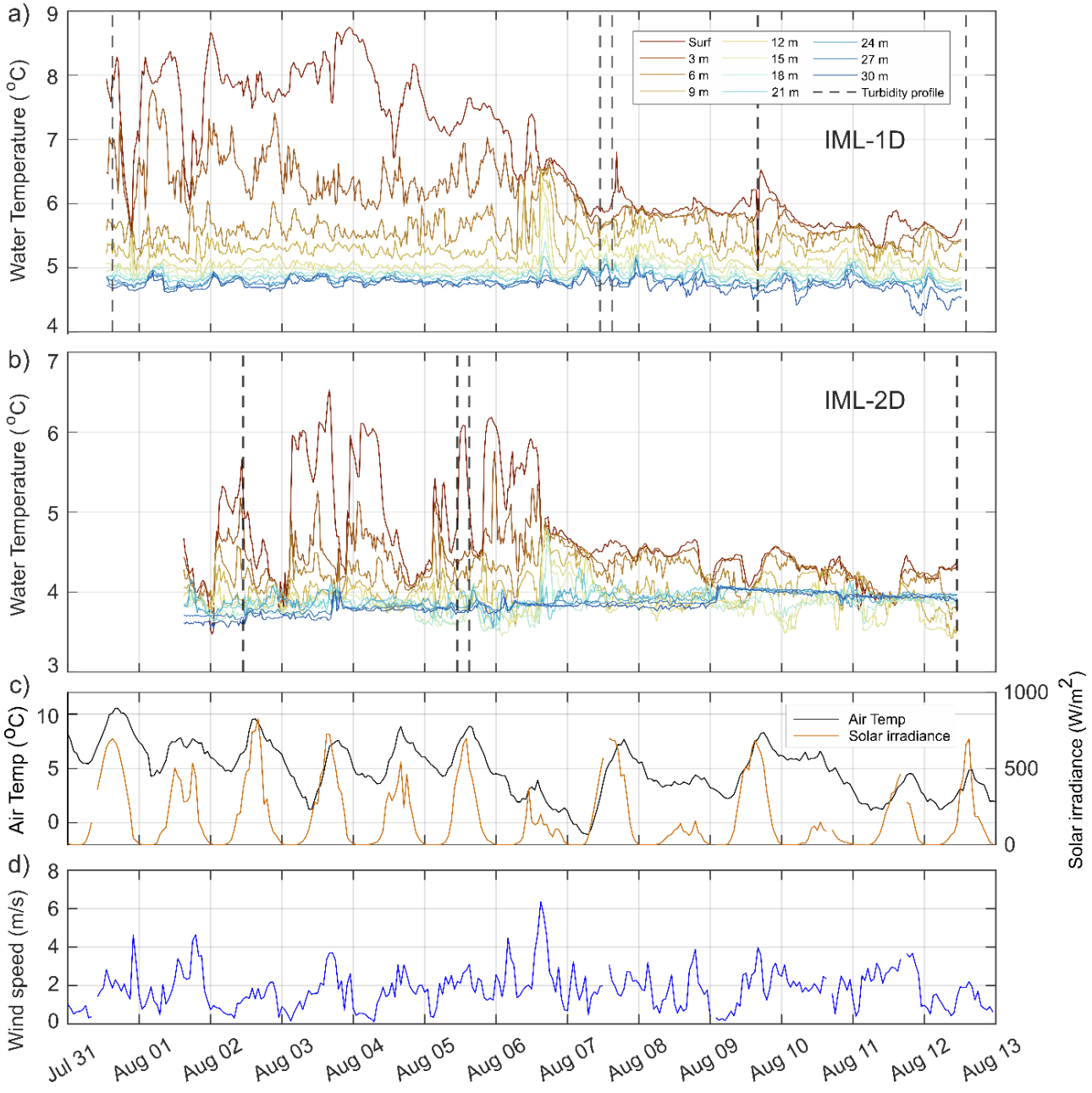


Figure 10. Lake temperature time series for IML-1D (a) and IML-2D (b) in early August 2025. Note the increased density of thermistors along each string, with loggers placed every 3 m. Black vertical dashed lines indicate the timing of turbidity profiles measurements (Fig. 11; Supplementary Table 1) at each thermistor string. (c) and (d) Land-based meteorological data for air temperature (black), solar radiation (orange) and wind speed (blue).

https://doi.org/10.5194/egusphere-2026-6324
Preprint. Discussion started: 26 November 2026
© Author(s) 2026. CC BY 4.0 License.

4.4 Turbidity profiles

IML-2 was the most turbid lake, with a depth-averaged median turbidity of 89.4 NTU (Nephelometric Turbidity Unit) at IML-2D and 90.2 NTU at IML-2B (Fig. 11). By comparison, the median turbidity of IML-1D was 51.0 NTU, whilst NGL had a median turbidity of just 0.2 NTU. There were also contrasting patterns in the depth-profiles of turbidity between lakes (Fig. 11). Turbidity remained constant at all depths at NGL-A and IML-1D; five turbidity profiles conducted on different days at IML-1D recorded consistent turbidity readings of between 45-53 NTU at all depths. By contrast, IML-2D displayed significantly higher turbidity at depth than towards the lake surface. Three out of four repeat profiles conducted at IML-2D were characterised by relatively stable turbidity readings of 70-80 NTU between the surface and 15 m depth, with gradually increasing turbidity with depth thereafter. Mean turbidity from these three profiles was 86.9 NTU (SD = 1.4 NTU) at 15 m depth, 99.7 NTU (SD = 4.6 NTU) at 21 m, and 144.0 NTU (SD = 18.9 NTU) at 27 m depth. The fourth profile from IML-2D, conducted at 11am on 12 August 2025, displayed markedly higher turbidity at the greatest depths (Fig. 11). Turbidity increased from 96.5 NTU at 9 m to 400.3 NTU at 30 m depth; more than double the magnitude of any other turbidity readings taken at the same location. Turbidity in the upper 15 m of the water column at IML-2B was relatively similar in magnitude to measurements from IML-2D, but, unlike at IML-2D, turbidity did not increase significantly at depth.

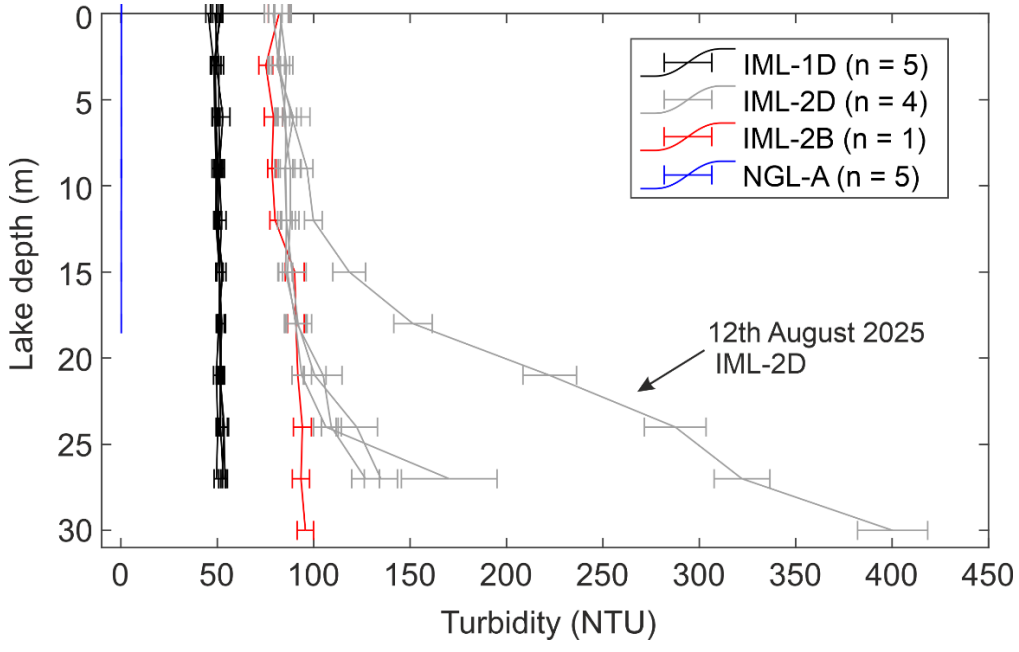


Figure 11. Turbidity profile measurements taken at IML-1D (black, n = 5), IML-2D (grey, n = 4), IML-2B (red, n = 1) and NGL-A (blue, n = 1). Measurements are displayed at 3 m depth intervals. Error bars indicate one standard deviation above and below the mean value at each depth (see Methods, Section 3.5). Dates and times of all turbidity profiles are shown in Supplementary Table 1.

https://doi.org/10.5194/egusphere-2026-6324
Preprint. Discussion started: 26 November 2026
© Author(s) 2026. CC BY 4.0 License.

4.5 Correlation analysis

We observe contrasting correlations between lake temperature and air temperature across the three lakes during summer 2024 (Fig. 12a). Both NGL and IML-1 display significant strong positive ($R > 0.7$, $p<0.05$) correlations between daily air temperature and lake temperature at the lake surface, with gradually decreasing correlation strength with depth (Fig. 12a). No statistically significant correlations were observed below 10 m depth. By contrast, IML-2 displays no statistically significant correlations in the uppermost 10 m of the water column, but shows negative correlations at depth (Fig. 12a). This pattern is observed across all three thermistor strings on IML-2, although negative correlations are only statistically significant at the deepest loggers on IML-2B and IML-2C.

Correlation analyses between lake temperature and solar radiation reveal similarly constrasting patterns (Fig. 12b). IML-1 and NGL display significant positive correlations in the top 5 m of the water column, with weaker non-significant positive correlations at depth, as observed with air temperature. However, correlation strengths at the lake surface ($R = 0.45 – 0.55$ for IML-1 and NGL) were slightly weaker than those observed for air temperature. At IML-2, lake temperature and solar radiation were negatively correlated at all depths, with the strongest correlations occuring in the deepest water (Fig. 12b); significant ($p < 0.05$) negative correlations of -0.26 (IML-2A), -0.55 (IML-2B) and -0.58 (IML-2C) were observed at the deepest thermistor of each string.

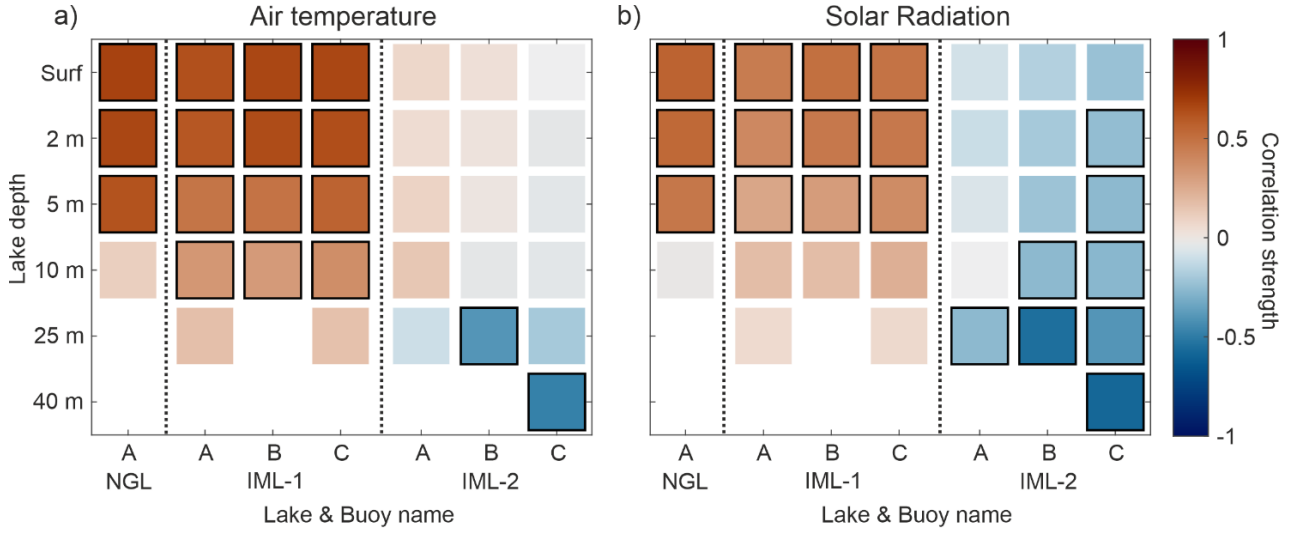


Figure 12. (a) Colour matrix displaying correlation strength (R) between daily mean air temperature and daily mean lake temperature during summer 2024 (10 July – 18 September 2024, n = 70). Each coloured square shows the correlation strength for that given thermistor string and lake depth. Black square outlines indicate statistically significant ($p < 0.05$) results. (b)

https://doi.org/10.5194/egusphere-2026-6324
Preprint. Discussion started: 26 November 2026
© Author(s) 2026. CC BY 4.0 License.

Equivalent matrix showing correlations between daily mean solar radiation and daily mean lake temeprature for the same time period.

5 Discussion

5.1 Summer lake behaviour

All three lakes were subject to a common atmopsheric forcing during summer months, characterised by relatively warm air temperatures, high solar radiation and sporadic high wind events. Lake temperature data from NGL provides a baseline response to this atmospheric forcing, whilst results from IML-1 and IML-2 highlight additional thermal variations likely driven by ice-marginal and glacial melt influences. Summer stratification of NGL and IML-1 were associated with periods of consistently low wind speeds, limiting vertical mixing of the water column. Our data suggest that wind speeds of >8 m/s were required to trigger full-depth mixing, as observed in late July 2024 (Fig. 5). Cooling phase mixing of NGL from 11 August 2024 appears to initially be wind-driven, with subsequent contiuous mixing driven by surface heat flux loss to the atmosphere as a result of steadily declining air temperatures during late August (Fig. 4).

The contrasting glacial settings of the three study lakes is likely the primary reason for the observed differences in summer lake temperatures. IML-1 and IML-2 receive ~0 °C meltwater inputs from subaqueous ice-front melting, iceberg calving, and overland or subglacial inflows, exerting a cooling effect on the lakes (Watson et al., 2020; Sugiyama et al., 2021). By contrast, NGL occupies a confined topographic basin isolated from the ice sheet, hence likely why its median depth-averaged summer 2024 temperature (9.41 °C) was significantly higher than that of IML-1 (5.05 °C) and IML-2 (3.39 °C). We find much clearer evidence for glacial influence on lake temperature than previous work in the Kangerlussuaq region, which found no significant difference in lake surface temperature between glacially-fed and groundwater-fed lakes (Burpee et al., 2018). However, the glacially-fed lakes studied by Burpee et al. (2018) comprised both ice-contact and non-ice contact lakes, whilst reported lake temperatures contained a mix of near-shore and lake centre measurements. These differences highlight the importance of documenting precise spatial and technical details of temperature data collection (such as exact logger locations and depths) alongside lake type, as these variables directly influence observed thermal dynamics. In particular, studies should clearly differentiate between ice-contact lakes, glacially-fed lakes not in contact with the ice sheet, and lakes with no glacial meltwater inputs (i.e. groundwater or catchment-fed only).

The lower temperatures in IML-2 relative to IML-1 are likely due to differences in geometry and/or glacial inputs. While the ice-lake contact length at IML-2 is nearly four times greater than at IML-1, this difference scales approximately proportionally with the lake area difference between the two lakes. Enhanced subaqeuous melt and calving inputs at IML-2 are hence distributed over a larger water mass, limiting their cooling effect. Since both lakes have relatively similar depth, we deem it unlikley that geometry is the primary driver of the temperature variability. Instead, turbidity data indicate distinct hydrological regimes between the two lakes. Turbidity is markedly higher in IML-2 than in IML-1, with profile data from IML-2D exhibiting

https://doi.org/10.5194/egusphere-2026-6324
Preprint. Discussion started: 26 November 2026
© Author(s) 2026. CC BY 4.0 License.

a persistent pattern of increasing turbidity with depth, periodically augmented by high-magnitude pulses near the lake bed (Fig. 11). Combined with thermal profile data, these elevated deep-water turbidities provide strong evidence for inputs of cold, sediment-rich subglacial meltwater that directly cool the basin. Turbidity data from IML-1D provide no indication of subglacial meltwater input. Instead, glacial inputs are inferred to originate primarily from overland flow or iceberg calving, both of which lack the high sediment loads characteristic of subglacial meltwater.

Lake turbidity differences, likely driven by variable glacial meltwater inputs, exert a fundamental control on thermal structure by altering solar radiation attenuation, hence influencing heat distribution (Hocking & Straškraba, 1999). At NGL, high water clarity and low turbidity enables shortwave radiation to penetrate several metres into the water column, establishing a thermocline at ~5–10 m depth during summer stratification (Fig. 5a). This aligns with regional observations from non-glacial lakes reporting average Secchi disk depths (a measure of water clarity) of 7.7 m (Burpee et al., 2018). By contrast, high turbidity at IML-1 and IML-2 restricts light penetration to the uppermost section of the water column, trapping heat near the surface and producing steep thermal gradients of 1–3 °C across the upper 5 m during stratification. Over shorter (hourly to daily) timescales, this solar heating is modulated by ice-marginal processes. While NGL displays smooth, sinusoidal diurnal surface temperature variations driven by air temperature and solar irradiance fluctuations, surface observations from IML-1 and IML-2 are often interrupted by erratic, high-frequency thermal fluctuations (up to several degrees per hour; Fig. 5). These are likely driven by calving events and localized iceberg meltout, as confirmed by time-lapse camera imagery showing frequent iceberg drift past thermistor string locations.

At greater lake depths, lake turbidity patterns and water column stability are influenced by the presence or absence of subglacial meltwater discharge. Our results indicate that the density structure of IML-2 is strongly influenced by these seasonal and episodic inputs of sediment-laden subglacial meltwater. During July 2024, deep water at IML-2A and IML-2B exhibited an anomalous thermal structure (Section 4.3.1) that cannot be explained by temperature-driven density variations alone, demonstrating that suspended sediment exerted a primary control on water column stability (Sugiyama et al., 2021). By early September 2024, as surface ablation and subglacial discharge likely waned (van As et al., 2018), conventional inverse thermal stratification was re-established. Observations at IML-2D from August 2025 further support this mechanism: during periods of limited subglacial flux (1 – 9 August, as inferred from turbidity and thermal data), the lake maintained a conventional, temperature-driven thermal structure (Fig. 10b). We hypothesize that the sudden deep-water temperature increase on 9 August 2025 (Fig. 10b) was triggered by a subglacial discharge pulse, which delivered turbid, dense water masses along the lake bed and disrupted vertical stratification. Although subglacial meltwater enters at near-freezing temperatures, the ~4 °C signature of the highly turbid deep layer between 9 – 12 August indicates significant entrainment of ambient water as the hyperpycnal plume plunged along the lake bed slope. These dynamics highlight how coupled variations in subglacial discharge volume, sediment load, and water temperature can dictate ice-marginal lake density structures over sub-hourly to daily timescales.

The contrasting associations we observe between lake temperature and air temperature/solar radiation during summer 2024 (Fig. 12) provides further evidence of differing hydrological regimes between IML-1 and IML-2. Whilst IML-1 and NGL displayed strong positive correlations near the surface with negligible association in deeper water, IML-2 had relatively strong

https://doi.org/10.5194/egusphere-2026-6324
Preprint. Discussion started: 26 November 2026
© Author(s) 2026. CC BY 4.0 License.

negative correlations (with both air temeprature and solar radiation) at depth. We hypothesize that these negative correlations at depth are due to increased subglacial meltwater input on warm, sunny days when ice sheet surface melt would be expected to be strongest. Widespread moulin and crevasse presence in low-elevation, marginal areas of the ice sheet provide direct pathways for the rapid transfer of meltwater from the surface to the bed of the ice sheet (Chandler et al., 2013; Clason et al., 2015). Whilst the residency time of meltwater varies seasonally depending on the configuration and efficiency of the subglacial drainage system, the establishment of efficient subglacial channels by July and August can result in the evacuation of surface derived meltwater on hourly timescales (Bartholomew et al., 2012). The negative correlations we observe at depth possibly indicate a sub-daily lag period between meltwater generation and subsequent subglacial input into IML-2. However, high turbidity recorded on 12 August 2025 followed two consecutive days of relatively low air temperatures (<5 °C; Fig. 10c), indicating a multi-day lag between meltwater production and evacuation into the lake.

5.2 Winter lake behaviour

During winter months, lake ice and overlying snow cover insulate the water column from atmospheric heat flux, preventing wind-driven mixing and restricting solar irradiance penetration (Kirillin et al., 2012; Oleksy & Richardson, 2024). Timelapse camera imagery suggests that the timing of snow cover onset and removal was key for determining when lake temperatures could respond to atmospheric forcing. Towards the surface, quasi-monthly variability in 2 m lake temperatures tracked large fluctuations in air temperature during spring (February to May). Warm air spells were observed to drive surface snowmelt (Fig. 9c), increasing ice transparency and allowing solar radiation to penetrate the upper water column. These transitions in surface conditions, rather than direct sensible heat exchange across the ice, were likely the primary cause of below-ice lake thermal changes. Solar radiation penetration likely also destabilised the water immediately below the surface ice, increasing heat flux from the relatively warm lake water towards the ice base via radiatively driven convection (Kirillin et al., 2012). This thermal sensitivity during spring was particularly pronounced at NGL where high water/ice clarity and deep light penetration enabled greater solar heat flux beneath the ice compared to the turbid ice-marginal lakes. Below the depth of solar penetration, water temperatures at NGL and IML-1 remained stable between mid-October 2024 and mid-May 2025 (Fig. 7) due to the absence of wind-driven mixing (Kirchner et al., 2024).

Glacial influences on ice-marginal lake temperatures are largely negated during the winter; overland and subglacial meltwater supply mostly cease due to the lack of ice sheet surface melting, whilst surface lake ice cover prevents calved icebergs from interacting with the lake water. Consequently, the thermal structure and absolute temperatures of all three lakes were very similar during winter: cryostratified (Yang et al., 2021), with near-surface (2 m) temperatures ranging between 0 and 2 °C and warmer temperatures of ~3 °C at depth. However, whilst IML-1 and NGL displayed stable temperatures at depth following ice-on, deeper waters in IML-2 progressivley cooled throughout the winter period, with notable hourly-to-daily variability (Fig. 7c). In the absence of atmospheric or lake surface influences on water tens of metres beneath thick surface ice, we suggest this was most likely caused by the gradual release of residually stored subglacial liquid meltwater into IML-2. Winter liquid

https://doi.org/10.5194/egusphere-2026-6324
Preprint. Discussion started: 26 November 2026
© Author(s) 2026. CC BY 4.0 License.

subglacial meltwater storage is widespread in west Greenland (Chu et al., 2016), and winter liquid water flow has been detected in a proglacial channel emerging from Issunguata Sermia (~20 km north of our study site), implying year-round meltwater storage and drainage (Pitcher et al., 2020). Whilst there is not thought to be a subglacial trough immediately beneath the ice flowing into IML-2 (Lindback et al., 2014), it is possible that subglacial channels flowing into IML-2 during summer remained partially open during winter, channeling residually stored meltwater from the wider Leverett basin. A sharp drop of ~0.15 °C at IML-2A-25m in late November 2024 (Fig. 7c), without coincident changes in lake temperatures above, was likely the result of a slug of subglacial meltwater being injected near the bottom of the lake.

5.3 Freezing and thawing period lake behaviour

During freezing and thaw transitions, thermal regimes at all lakes were governed by a coupled interaction between atmospheric forcing, glacial inputs, and evolving surface ice conditions. Analysis of timelapse imagery from IML-1 highlights the particularly strong influence that evolving surface conditions had on lake temperatures during thawing in spring 2025 (Fig. 12), though it's likely surface evolution had similarly high influences at the other study lakes. At IML-1, spring melting of overlying snow cover initiated rapid lake warming at 2 m depth, as the removal of snow allowed shortwave solar radiation to penetrate the surface ice. Subsequent surface meltwater ponding likely further accelerated ice thinning by lowering surface albedo and enhancing radiative absorption (Kirchner et al., 2024). Liquid meltwater and slush infiltration may also have exploited surface fractures, potentially weakening the lake ice via processes of freeze-thaw and fracture propagation. As perimeter thawing established open-water channels along the lake margins, direct atmospheric heat exchange resumed (Kirillin et al., 2012). Together, these evolving surface processes, driven by continuously rising air temperatures and increasing solar radiation strength, facilitated progressive heat transfer into the upper water column throughout late spring until the lake became entirely free of surface ice. Constraining the relationship between lake thermal dynamics and seasonal lake ice cover is critical, as the latter has been shown to influence both calving rates and styles (Mallalieu et al., 2020).

6 Conclusions

This study provides the first continuous, high-resolution in-situ dataset of ice-marginal lake temperatures in Greenland. Our results demonstrate that Greenlandic ice-marginal lakes can exhibit relatively warm water temperatures and stratified thermal structures, with surface temperatures up to 8 °C proximal to the ice front and temperatures above 4 °C persisting throughout the water column. These observations indicate that subaqueous melt rates in some ice-marginal settings may be substantially higher than previously assumed, contrasting with cold-water systems (<1 °C) recorded in southern Greenland (Vacek et al., 2026). Significantly, enhanced thermal undercutting at the ice front from warm surface waters could directly influence calving rates and ice-margin dynamics. Expanding in-situ temperature monitoring across different sectors of Greenland and other glaciated regions is therefore critical to evaluate the regional representativeness of these relatively warm thermal regimes.

https://doi.org/10.5194/egusphere-2026-6324
Preprint. Discussion started: 26 November 2026
© Author(s) 2026. CC BY 4.0 License.

Priority should be given to establishing relationships between surface thermal observations and subsurface profile dynamics to enable robust remote sensing scaling. Future work could also couple thermal measurements with quantified rates of subaqueous melt and calving to investigate how lake stratification influences calving style, frequency and magnitude.

The distinct thermal dynamics between our two ice-marginal study lakes demonstrate the strong influence of glacial hydrological regimes on lake structure. At IML-2, sediment-laden subglacial meltwater altered water column density and cooled the basin during summer, while winter observations indicate persistent subglacial inputs driven by residual meltwater release, causing gradual cooling at depth. In contrast, thermal measurements from adjacent IML-1 revealed extended periods of summer stratification, with highly stable lake temperatures at depth through winter. This highlights the marked heterogeneity in thermal characteristics that can exist between ice-marginal lakes across small spatial scales. Crucially, these findings demonstrate that assigning uniform, near-freezing lake temperatures in ice-sheet models would oversimplify ice-marginal environments. Further empirical understanding is therefore required before ice-marginal lake thermal processes can be accurately parameterised within large-scale projections of ice-sheet evolution.

Data availability

All field measurements of lake temperature, meteorological conditions and turbidity are available via Zenodo at https://doi.org/10.5281/zenodo.23214785 (Tuckett, 2026). Data from the Programme for Monitoring of the Greenland Ice Sheet (PROMICE) are provided by the Geological Survey of Denmark and Greenland (GEUS) at http://www.promice.dk. PlanetScope SuperDove imagery is proprietary data provided by Planet Labs PBC and can be accessed upon registration and subject to licensing via Planet Explorer (https://www.planet.com/explorer/).

Author contributions

PAT, DMR and DJQ designed the study. PAT led the field data collection, interpreted the results, and wrote the manuscript. Fieldwork to deploy, maintain and retrieve sensor data was carried out by PAT, CMH, ACS, DJQ, HFB, JA, JM, LDR, JLS and DMR. CJR, RIW, LC, NM and WW contributed to data interpretation and analysis. All authors contributed to editing of the final manuscript.

https://doi.org/10.5194/egusphere-2026-6324
Preprint. Discussion started: 26 November 2026
© Author(s) 2026. CC BY 4.0 License.

Competing interests

The authors declare that they have no conflict of interest.

Disclaimer

Publisher's note: Copernicus Publications remains neutral with regard to jurisdictional claims made in the text, published maps, institutional affiliations, or any other geographical representation in this paper. While Copernicus Publications makes every effort to include appropriate place names, the final responsibility lies with the authors. Views expressed in the text are those of the authors and do not necessarily reflect the views of the publisher.

Acknowledgements

We acknowledge field-based logistical support from Chris Sørenson at Kangerlussuaq International Science Support, and Air Greenland for helicopter support. We acknowledge Planet Labs PBC for providing access to PlanetScope SuperDove imagery through the Education and Research Program.

Financial support

This work was funded by a NERC grant (NE/X013537/1) awarded to DMR, DJQ, CJM and RIW. CMH acknowledges funding from a UKRI NERC PhD studentship (NE/S007458/1). We thank the Tempcon sponsorship programme for financial support purchasing thermistor loggers.

7 References

Bartholomew, I., Nienow, P., Sole, A., Mair, D., Cowton, T., & King, M. A. (2012). Short-term variability in Greenland Ice Sheet motion forced by time-varying meltwater drainage: Implications for the relationship between subglacial drainage system behavior and ice velocity. *Journal of Geophysical Research: Earth Surface*, *117*(F3). https://doi.org/10.1029/2011JF002220

Boehrer, B., & Schultze, M. (2008). Stratification of lakes. *Reviews of Geophysics*, *46*(2). https://doi.org/10.1029/2006RG000210

Burpee, B. T., Anderson, D., & Saros, J. E. (2018). Assessing ecological effects of glacial meltwater on lakes fed by the Greenland Ice Sheet: The role of nutrient subsidies and turbidity. *Arctic, Antarctic, and Alpine Research*, *50*(1), S100019. https://doi.org/10.1080/15230430.2017.1420953

https://doi.org/10.5194/egusphere-2026-6324
Preprint. Discussion started: 26 November 2026
© Author(s) 2026. CC BY 4.0 License.

Carrea, L., Merchant, C. J., Woolway, R. I., & McCarroll, N. (2025). Factors influencing lake surface water temperature variability in West Greenland and the role of the ice sheet. *The Cryosphere*, *19*(8), 3139–3158. https://doi.org/10.5194/tc-19-3139-2025

Carrivick, J. L., How, P., Lea, J. M., Sutherland, J. L., Grimes, M., Tweed, F. S., Cornford, S., Quincey, D. J., & Mallalieu, J. (2022). Ice-Marginal Proglacial Lakes Across Greenland: Present Status and a Possible Future. *Geophysical Research Letters*, *49*(12), e2022GL099276. https://doi.org/10.1029/2022GL099276

Carrivick, J. L., & Quincey, D. J. (2014). Progressive increase in number and volume of ice-marginal lakes on the western margin of the Greenland Ice Sheet. *Global and Planetary Change*, *116*, 156–163. https://doi.org/10.1016/j.gloplacha.2014.02.009

Carrivick, J. L., Tweed, F. S., Ng, F., Quincey, D. J., Mallalieu, J., Ingeman-Nielsen, T., Mikkelsen, A. B., Palmer, S. J., Yde, J. C., Homer, R., Russell, A. J., & Hubbard, A. (2017). Ice-Dammed Lake Drainage Evolution at Russell Glacier, West Greenland. *Frontiers in Earth Science*, *5*. https://doi.org/10.3389/feart.2017.00100

Carrivick, J. L., Tweed, F. S., Sutherland, J. L., & Mallalieu, J. (2020). Toward Numerical Modeling of Interactions Between Ice-Marginal Proglacial Lakes and Glaciers. *Frontiers in Earth Science*, *8*. https://doi.org/10.3389/feart.2020.577068

Chandler, D. M., Wadham, J. L., Lis, G. P., Cowton, T., Sole, A., Bartholomew, I., Telling, J., Nienow, P., Bagshaw, E. B., Mair, D., Vinen, S., & Hubbard, A. (2013). Evolution of the subglacial drainage system beneath the Greenland Ice Sheet revealed by tracers. *Nature Geoscience*, *6*(3), 195–198. https://doi.org/10.1038/ngeo1737

Chu, W., Schroeder, D. M., Seroussi, H., Creyts, T. T., Palmer, S. J., & Bell, R. E. (2016). Extensive winter subglacial water storage beneath the Greenland Ice Sheet. *Geophysical Research Letters*, *43*(24), 12,484-12,492. https://doi.org/10.1002/2016GL071538

Clason, C. C., Mair, D. W. F., Nienow, P. W., Bartholomew, I. D., Sole, A., Palmer, S., & Schwanghart, W. (2015). Modelling the transfer of supraglacial meltwater to the bed of Leverett Glacier, Southwest Greenland. *The Cryosphere*, *9*(1), 123–138. https://doi.org/10.5194/tc-9-123-2015

Dye, A., Bryant, R., Falcini, F., Mallalieu, J., Dimbleby, M., Beckwith, M., Rippin, D., & Kirchner, N. (2025). Warm proglacial lake temperatures and thermal undercutting enhance rapid retreat of an Arctic glacier. *The Cryosphere*, *19*(10), 4471–4486. https://doi.org/10.5194/tc-19-4471-2025

Ellis, C. R., Stefan, H. G., & Gu, R. (1991). Water temperature dynamics and heat transfer beneath the ice cover of a lake. *Limnology and Oceanography*, *36*(2), 324–334. https://doi.org/10.4319/lo.1991.36.2.0324

Fausto, R. S., How, P., Vandecrux, B., Lund, M. C., Box, J. E., Mankoff, K. D., Andersen, S. B., van As, D., Bahbah, R., Citterio, M., Colgan, W., Jakobsgaard, H. T., Karlsson, N. B., Kjeldsen, K. K., Larsen, S. H., Olsen, C., Oraschewski, F. M., Rutishauser, A., Shields, C. L., … Ahlstrøm, A. P. (2026). PROMICE | GC-NET automatic weather station data. *Earth System Science Data*, *18*(4), 2829–2873. https://doi.org/10.5194/essd-18-2829-2026

https://doi.org/10.5194/egusphere-2026-6324
Preprint. Discussion started: 26 November 2026
© Author(s) 2026. CC BY 4.0 License.

Gardner, A. S., Greene, C. A., Kennedy, J. H., Fahnestock, M. A., Liukis, M., López, L. A., Lei, Y., Scambos, T. A., & Dehecq, A. (2025). ITS_LIVE global glacier velocity data in near-real time. *The Cryosphere*, *19*(9), 3517–3533. https://doi.org/10.5194/tc-19-3517-2025

Greenland Ecosystem Monitoring. (2020). *BioBasis Nuuk—Lakes—Water temperature* (Version 1.0) [Dataset]. Greenland Ecosystem Monitoring. https://doi.org/10.17897/BKTY-J070

Hanna, E., Box, J. E., Fettweis, X., van den Broeke, M. R., Wake, L., Luu, L., Maddison, J., Mote, T., Mottram, R., Noël, B., Preece, J., Topál, D., Trusel, L., & van der Laan, L. N. (2026). Past, present and future Greenland Ice Sheet surface melt, 1500–2200 CE. *Nature Reviews Earth & Environment*, 1–17. https://doi.org/10.1038/s43017-026-00800-3

Harpur, C. M., Smith, M. W., Carrivick, J. L., Quincey, D. J., & Taylor, L. (2026). Ice-marginal proglacial lakes enhance outlet glacier velocities across Greenland. *Communications Earth & Environment*, *7*(1), 287. https://doi.org/10.1038/s43247-026-03363-9

Hocking, G. C., & Straskraba, M. (1999). The Effect of Light Extinction on Thermal Stratification in Reservoirs and Lakes. *International Review of Hydrobiology*, *84*(6), 535–556. https://doi.org/10.1002/iroh.199900046

How, P., Messerli, A., Mätzler, E., Santoro, M., Wiesmann, A., Caduff, R., Langley, K., Bojesen, M. H., Paul, F., Kääb, A., & Carrivick, J. L. (2021). Greenland-wide inventory of ice marginal lakes using a multi-method approach. *Scientific Reports*, *11*(1), 4481. https://doi.org/10.1038/s41598-021-83509-1

How, P., Petersen, D., Kjeldsen, K. K., Raundrup, K., Karlsson, N. B., Messerli, A., Rutishauser, A., Carrivick, J. L., Lea, J. M., Fausto, R. S., Ahlstrøm, A. P., & Andersen, S. B. (2025). The Greenland Ice-Marginal Lake Inventory Series from 2016 to 2023. *Earth System Science Data*, *17*(11), 6331–6351. https://doi.org/10.5194/essd-17-6331-2025

Kettle, H., Thompson, R., Anderson, N. J., & Livingstone, D. M. (2004). Empirical modeling of summer lake surface temperatures in southwest Greenland. *Limnology and Oceanography*, *49*(1), 271–282. https://doi.org/10.4319/lo.2004.49.1.0271

Kirchner, N., Weckström, J., Jansen, J., Schenk, F., Barnett, J., Granebeck, A., Leppäranta, M., & Korhola, A. (2024). Water temperature, mixing, and ice phenology in the arctic–alpine Lake Darfáljávri (Lake Tarfala), northern Sweden. *Arctic, Antarctic, and Alpine Research*, *56*(1), 2287704. https://doi.org/10.1080/15230430.2023.2287704

Kirillin, G., Leppäranta, M., Terzhevik, A., Granin, N., Bernhardt, J., Engelhardt, C., Efremova, T., Golosov, S., Palshin, N., Sherstyankin, P., Zdorovennova, G., & Zdorovennov, R. (2012). Physics of seasonally ice-covered lakes: A review. *Aquatic Sciences*, *74*(4), 659–682. https://doi.org/10.1007/s00027-012-0279-y

Kirkbride, M. P., & Warren, C. R. (1997). Calving processes at a grounded ice cliff. *Annals of Glaciology*, *24*, 116–121. https://doi.org/10.3189/S0260305500012039

Liang, S. (2001). Narrowband to broadband conversions of land surface albedo I: Algorithms. *Remote Sensing of Environment*, *76*(2), 213–238. https://doi.org/10.1016/S0034-4257(00)00205-4

https://doi.org/10.5194/egusphere-2026-6324
Preprint. Discussion started: 26 November 2026
© Author(s) 2026. CC BY 4.0 License.

Lindback, K., Pettersson, R., Doyle, S. H., Helanow, C., Jansson, P., Kristensen, S. S., Stenseng, L., Forsberg, R., & Hubbard, A. L. (2014). High-resolution ice thickness and bed topography of a land-terminating section of the Greenland Ice Sheet. *Earth System Science Data*, *6*(2), 331–338. https://doi.org/10.5194/essd-6-331-2014

Mallalieu, J., Carrivick, J. L., Quincey, D. J., & Raby, C. L. (2021). Ice-marginal lakes associated with enhanced recession of the Greenland Ice Sheet. *Global and Planetary Change*, *202*, 103503. https://doi.org/10.1016/j.gloplacha.2021.103503

Mallalieu, J., Carrivick, J. L., Quincey, D. J., & Smith, M. W. (2020). Calving Seasonality Associated With Melt-Undercutting and Lake Ice Cover. *Geophysical Research Letters*, *47*(8), e2019GL086561. https://doi.org/10.1029/2019GL086561

Minowa, M., Schaefer, M., & Skvarca, P. (2023). Effects of topography on dynamics and mass loss of lake-terminating glaciers in southern Patagonia. *Journal of Glaciology*, *69*(278), 1580–1597. https://doi.org/10.1017/jog.2023.42

Minowa, M., Sugiyama, S., Sakakibara, D., & Skvarca, P. (2017). Seasonal Variations in Ice-Front Position Controlled by Frontal Ablation at Glaciar Perito Moreno, the Southern Patagonia Icefield. *Frontiers in Earth Science*, *5*. https://doi.org/10.3389/feart.2017.00001

Oleksy, I. A., & Richardson, D. C. (2024). *Shorter Ice Duration and Changing Phenology Influence Under-Ice Lake Temperature Dynamics*. https://doi.org/10.1029/2024JG008382

Pitcher, L. H., Smith, L. C., Gleason, C. J., Miège, C., Ryan, J. C., Hagedorn, B., van As, D., Chu, W., & Forster, R. R. (2020). Direct Observation of Winter Meltwater Drainage From the Greenland Ice Sheet. *Geophysical Research Letters*, *47*(9), e2019GL086521. https://doi.org/10.1029/2019GL086521

Röhl, K. (2006). Thermo-erosional notch development at fresh-water-calving Tasman Glacier, New Zealand. *Journal of Glaciology*, *52*(177), 203–213. https://doi.org/10.3189/172756506781828773

Ross, N., Sole, A. J., Livingstone, S. J., Igneczi, Á., & Morlighem, M. (2018). Near-margin ice thickness and subglacial water routing, Leverett Glacier, Greenland. *Arctic, Antarctic, and Alpine Research*, *50*(1), S100007. https://doi.org/10.1080/15230430.2017.1420949

Saros, J. E., Northington, R. M., Osburn, C. L., Burpee, B. T., & John Anderson, N. (2016). Thermal stratification in small arctic lakes of southwest Greenland affected by water transparency and epilimnetic temperatures. *Limnology and Oceanography*, *61*(4), 1530–1542. https://doi.org/10.1002/lno.10314

Scoffield, A. C., Quincey, D. J., Kerr, N. R., Rowan, A. V., Carrivick, J. L., Woolway, R. I., Khanal, N., Watson, C. S., & Cook, S. J. (2025). Monsoon and Glacial Meltwater Input Drive Seasonal Cooling of a Himalayan Ice-Contact Lake. *Water Resources Research*, *61*(11), e2024WR039155. https://doi.org/10.1029/2024WR039155

Sugiyama, S., Minowa, M., Fukamachi, Y., Hata, S., Yamamoto, Y., Sauter, T., Schneider, C., & Schaefer, M. (2021). Subglacial discharge controls seasonal variations in the thermal structure of a glacial lake in Patagonia. *Nature Communications*, *12*(1), 6301. https://doi.org/10.1038/s41467-021-26578-0

https://doi.org/10.5194/egusphere-2026-6324
Preprint. Discussion started: 26 November 2026
© Author(s) 2026. CC BY 4.0 License.

Sugiyama, S., Minowa, M., Sakakibara, D., Skvarca, P., Sawagaki, T., Ohashi, Y., Naito, N., & Chikita, K. (2016). Thermal structure of proglacial lakes in Patagonia. *Journal of Geophysical Research: Earth Surface*, *121*(12), 2270–2286. https://doi.org/10.1002/2016JF004084

Sugiyama, S., Minowa, M., & Schaefer, M. (2019). Underwater Ice Terrace Observed at the Front of Glaciar Grey, a Freshwater Calving Glacier in Patagonia. *Geophysical Research Letters*, *46*(5), 2602–2609. https://doi.org/10.1029/2018GL081441

Sutherland, J. L., Carrivick, J. L., Gandy, N., Shulmeister, J., Quincey, D. J., & Cornford, S. L. (2020). Proglacial Lakes Control Glacier Geometry and Behavior During Recession. *Geophysical Research Letters*, *47*(19), e2020GL088865. https://doi.org/10.1029/2020GL088865

Truffer, M., & Motyka, R. J. (2016). Where glaciers meet water: Subaqueous melt and its relevance to glaciers in various settings. *Reviews of Geophysics*, *54*(1), 220–239. https://doi.org/10.1002/2015RG000494

Tuckett, P. (2026). High resolution monitoring of Greenlandic Ice-marginal Lakes [Dataset]. Zenodo. https://doi.org/10.5281/zenodo.23214785

Vacek, F., Nick, F. M., Benn, D., Zwarts, M. P. A., Immerzeel, W., & van de Wal, R. S. W. (2026). Contrasting dynamics of lake- and marine-terminating glaciers under same climatic conditions. *The Cryosphere*, *20*(7), 3827–3845. https://doi.org/10.5194/tc-20-3827-2026

van As, D., Hasholt, B., Ahlstrøm, A. P., Box, J. E., Cappelen, J., Colgan, W., Fausto, R. S., Mernild, S. H., Mikkelsen, A. B., Noël, B. P. Y., Petersen, D., & van den Broeke, M. R. (2018). Reconstructing Greenland Ice Sheet meltwater discharge through the Watson River (1949–2017). *Arctic, Antarctic, and Alpine Research*, *50*(1), S100010. https://doi.org/10.1080/15230430.2018.1433799

Warren, C., Benn, D., Winchester, V., & Harrison, S. (2001). Buoyancy-driven lacustrine calving, Glaciar Nef, Chilean Patagonia. *Journal of Glaciology*, *47*(156), 135–146. https://doi.org/10.3189/172756501781832403

Warren, C. R., & Kirkbride, M. P. (1998). Temperature and bathymetry of ice-contact lakes in Mount Cook National Park, New Zealand. *New Zealand Journal of Geology and Geophysics*, *41*(2), 133–143. https://doi.org/10.1080/00288306.1998.9514797

Warren, C. R., & Kirkbride, M. P. (2003). Calving speed and climatic sensitivity of New Zealand lake-calving glaciers. *Annals of Glaciology*, *36*, 173–178. https://doi.org/10.3189/172756403781816446

Watson, C. S., Kargel, J. S., Shugar, D. H., Haritashya, U. K., Schiassi, E., & Furfaro, R. (2020). Mass Loss From Calving in Himalayan Proglacial Lakes. *Frontiers in Earth Science*, *7*. https://doi.org/10.3389/feart.2019.00342

Yang, B., Wells, M. G., McMeans, B. C., Dugan, H. A., Rusak, J. A., Weyhenmeyer, G. A., Brentrup, J. A., Hrycik, A. R., Laas, A., Pilla, R. M., Austin, J. A., Blanchfield, P. J., Carey, C. C., Guzzo, M. M., Lottig, N. R., MacKay, M. D., Middel, T. A., Pierson, D. C., Wang, J., & Young, J. D. (2021). A New Thermal Categorization of Ice-Covered Lakes. *Geophysical Research Letters*, *48*(3), e2020GL091374. https://doi.org/10.1029/2020GL091374